SANDIA REPORT
SAND2020-3824
Printed April 2020

Sandia National Laboratories

High Altitude Electromagnetic Pulse Testing of Photovoltaic Modules

Tyler Bowman
Jack Flicker
Ross Guttromson
Matthew Halligan
Rodrigo Llanes
Michael Ropp
Bruce King
Charles Robinson

Prepared by
Sandia National Laboratories
Albuquerque, New Mexico
87185 and Livermore,
California 94550

Issued by Sandia National Laboratories, operated for the United States Department of Energy by National Technology & Engineering Solutions of Sandia, LLC.

Available to DOE and DOE contractors from
U.S. Department of Energy
Office of Scientific and Technical Information
P.O. Box 62
Oak Ridge, TN 37831

Telephone: (865) 576-8401
Facsimile: (865) 576-5728
E-Mail: reports@osti.gov
Online ordering: http://www.osti.gov/scitech

Available to the public from
U.S. Department of Commerce
National Technical Information Service
5301 Shawnee Rd
Alexandria, VA 22312

Telephone: (800) 553-6847
Facsimile: (703) 605-6900
E-Mail: orders@ntis.gov
Online order: https://classic.ntis.gov/help/order-methods/

ABSTRACT

This report details the test setup, process, and results for radiated susceptibility testing of multicrystalline silicon photovoltaic (PV) modules as part of the EMP-Resilient Electric Grid Grand Challenge Laboratory Directed Research and Development (LDRD) project at Sandia National Laboratories. Testing was conducted over October 10-17, 2019, where 8 photovoltaic modules were exposed to E1 transient pulses with peak field levels up to 100 kV/m. Modules were terminated in a resistive load representing connected components. State of health testing conducted via I-V curve tracing of the photovoltaic modules showed no observable loss of device function due to large electric field transients. Differential mode currents were measured on the order of 10's of amps for up to a microsecond following the radiated field pulse. Common mode currents took the form of a damped sinusoid with a maximum peak of 10's to 100's of amps with a resonance near 60 MHz.

ACKNOWLEDGEMENTS

The authors wish to thank the following individuals for their contributions:

- Experimental Support
  - John Brown
  - Tyler Fronk
  - Steve Tullar
  - Forest White
- Technical Support
  - Alfred Baughman
  - Leonard Martinez
- Reviewers
  - Steve Glover

CONTENTS

LIST OF FIGURES

LIST OF TABLES

This page left blank

EXECUTIVE SUMMARY

A high-altitude electromagnetic pulse (HEMP) event is an artifact of a nuclear explosion detonated high in the atmosphere. Such explosions can be designed to minimize mechanical damage while maximizing electromagnetic pulses, which can damage electrical and electronic equipment. There is a possibility of a HEMP event occurring over the US, although the pervasiveness of consequences to the power grid from this event are presently unknown.

Sandia National Laboratories has launched a three-part multi-year investigation into this topic area. The approach uses three fundamental steps to characterize the consequences of HEMP for electric power generation and delivery. The first step is to evaluate the probability of failure and associated failure modes of select grid components as a function of magnitude and polarization of the EMP. The second is to sample these distributions to determine a single possible HEMP scenario to grid components. The last step will impose the failure conditions on a dynamic grid model, which includes limited system protection, and determine the short and long-term survivability of load delivery. This work addresses the first of the three steps, with focus on the potential vulnerability of photovoltaic (PV) systems to HEMP.

Testing was accomplished by insulting PV modules with an incident Transverse Electromagnetic (TEM) wave of increasing electric field strengths. Between each insult, the PV system's state of health (SOH) was measured to ensure it had not failed or degraded in performance. This cycle was repeated at increasing levels of TEM intensity ($|E_{radiated}|$) until the PV module failed or reached an unrealistically high electric field level. The process was repeated for several modules, and the resulting data were used to model component failure by constructing a Cumulative Density Function that is conditional on the TEM insult magnitude. Results in this statistical form allow a user to understand the component vulnerability across a variety of conditions. No direct failures of PV modules were observed during the testing of this report. Instead, a performance metric (fill factor) was used to determine any change in performance. It's important to note that this report only covers testing of the DC PV module and not the DC-DC converter or DC-AC inverter systems to which it is normally connected. These connected devices are potentially vulnerable to HEMP but will be addressed in separate testing.

The failure CDF of the PV modules, conditional on $0kV/m<|E_{radiated}|<50kV/m$ is equal to 0 (notes 1,2). Only a PV module performance CDF was generated in this work.

Notes:

1. 50kV/m was selected as the highest likely E-field expected from a HEMP. Higher field values were tested in this work to determine if point-of-failure of the PV modules could be reached.
2. Most of the testing reported here used a single orientation of the PV module with respect to the E-field polarization. Other module orientations may have increased susceptibility but are only addressed with single test cases here.

ACRONYMS AND DEFINITIONS

Abbreviation	Definition
CT	Current Transformer
CW	Continuous Wave
DUT	Device Under Test
E-field	Electric field
E1	Early-time HEMP
EL	Electroluminescence
EMES	Electromagnetic Environments Simulator
EMP	Electromagnetic Pulse
HEMP	High-altitude Electromagnetic Pulse
I-V	Current-voltage
LDRD	Laboratory Directed Research and Development
LED	Light-emitting diode
PSEL	Photovoltaic Systems Evaluation Laboratory
PV	Photovoltaic
RF	Radio Frequency
SNL	Sandia National Laboratories
SOH	State of health
TEM	Transverse Electromagnetic

1. INTRODUCTION

A High-Altitude Electromagnetic Pulse (HEMP) is an electromagnetic event caused by the detonation of a nuclear weapon at high altitudes. This event creates an electromagnetic pulse potentially capable of disrupting many electrical and electronic systems essential to life within the United States. A HEMP attack poses a serious threat to the well-being and security of the nation, including the electrical grid, but the exact vulnerabilities are not yet known. Therefore, it is desirable to study the impacts that an electromagnetic wave originating from a HEMP would have on the electrical grid.

This report covers a series of radiated susceptibility tests seeking to address the effect that a HEMP would have on multicrystalline silicon photovoltaic modules, also known as solar modules or solar panels. Solar power has become increasingly common as a renewable energy source for alternative power generation in the grid and for individual end-user power. The failure of one or more solar power generation stations during a HEMP event becomes a greater liability as more power generation is being shifted to these sources. As such, it is vital to identify any potential vulnerability that may exist within PV devices in response to HEMP.

A series of tests was conducted at the Sandia National Laboratories' (SNL) Electromagnetic Environments Simulator (EMES) facility to assess the susceptibility of PV modules to an EMP incident wave. Tests consisted of exposing the PV modules to a simulated early-time HEMP (E1) incident wave and comparing the module state of health (SOH) before and after each insult. A representative load was attached to the module to emulate the input impedance looking from the module into connected components.

2. EXPERIMENTAL OVERVIEW

2.1. Objectives

The primary objective of this test was to assess the vulnerability of the solar cells in multicrystalline silicon PV modules to HEMP transients. Individual modules were exposed to transient electric fields with a rise time of 2.4 ns and a pulse width of 37 ns with increasing peak values. The module state of health was measured after EMP environment exposures. A baseline 50 kV/m peak field strength limit was considered for a nominal maximum EMP environment, which is the standard E1 limit defined by international standards [1]. Following testing of the first module up to 50 kV/m, the testing range was increased to higher fields with a 100 kV/m maximum to determine if PV modules failed for margin test levels.

A secondary objective of this test was to quantify the electromagnetic coupling to the multicrystalline silicon PV modules that can be used for follow-on testing with PV inverters. Cable current measurements were performed to quantify common-mode (current traveling parallel through the signal and return path) and differential-mode (current traveling on the signal path and returning on the return path) currents that would normally flow through an inverter from a single module. The motivation for the current measurement is that a significant coupled pulse could potentially damage a regulator and inverter connected to the PV module, which would constitute a failure in power generation. The cumulative effect on inverters fed by more than one PV module in series and coupling to PV modules with materials other than multicrystalline silicon were not investigated in this test series.

2.2. Test Facility

EMES at SNL is a large transverse electromagnetic (TEM) cell designed to create uniform, planar electromagnetic waves in a working volume in which test objects are placed. EMES is typically used for electromagnetic transfer function measurements such as effective cable length and shielding effectiveness measurements, in addition to test article susceptibility measurements. Two different radio frequency (RF) feeds allow EMES to be operated in continuous wave (CW) or pulsed operations. For pulsed operation, a voltage pulser connects a series of charged capacitors to the center conductor of the TEM cell. The capacitors discharge across a peaking capacitor to send an electromagnetic pulse, or 'shot,' toward the test article. The resulting incident plane waves in the working volume are linearly polarized in the vertical direction. A diagram of the EMES facility is shown in Figure 2-1.

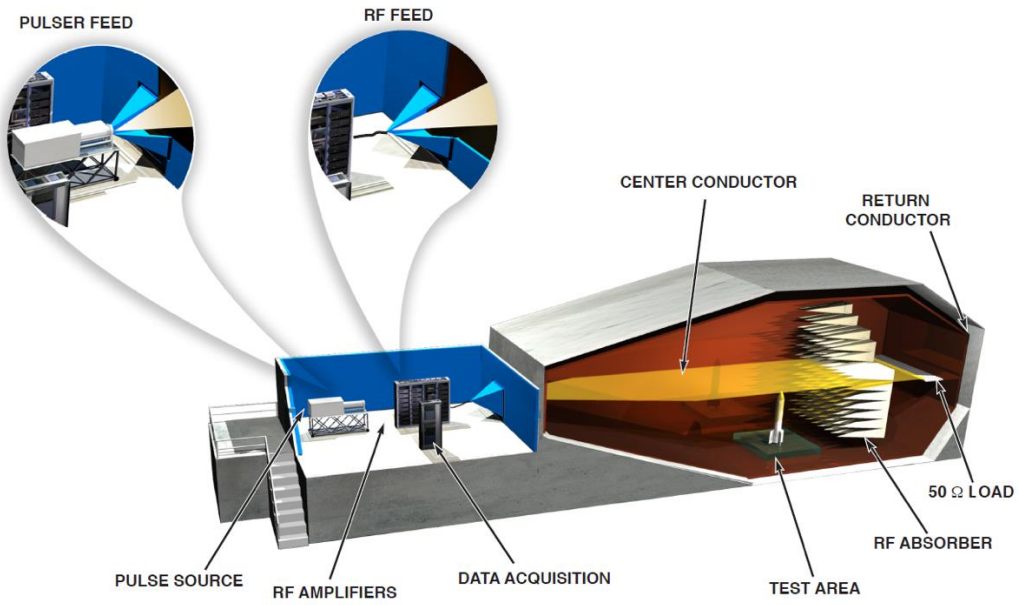

Figure 2-1. EMES cross-sectional diagram.

Power injected into the EMES working volume is absorbed by a combination of 4 m RF absorbers in Figure 2-2a and parallel resistor strings connecting the center conductor to the return conductor in Figure 2-2b. There are 52 parallel resistor strings of approximately 2600 Ω each, providing an equivalent load of 50 Ω. Below a few megahertz, the 50 Ω parallel-resistor load dissipates most of the injected power in the working volume. Above a few 10's of megahertz the RF absorbers dissipate most of the injected power in the working volume. In the transition frequency region above a few megahertz and below a few 10's of megahertz the injected power is dissipated by a combination of the load resistors and RF absorbers. The RF absorbers also serve to dampen higher order modes (non-transverse electromagnetic waves or cavity modes) induced in the facility when the facility becomes electrically large. These absorbers are supported by a non-metallic support structure to mitigate absorber degradation as seen in Figure 2-2a.

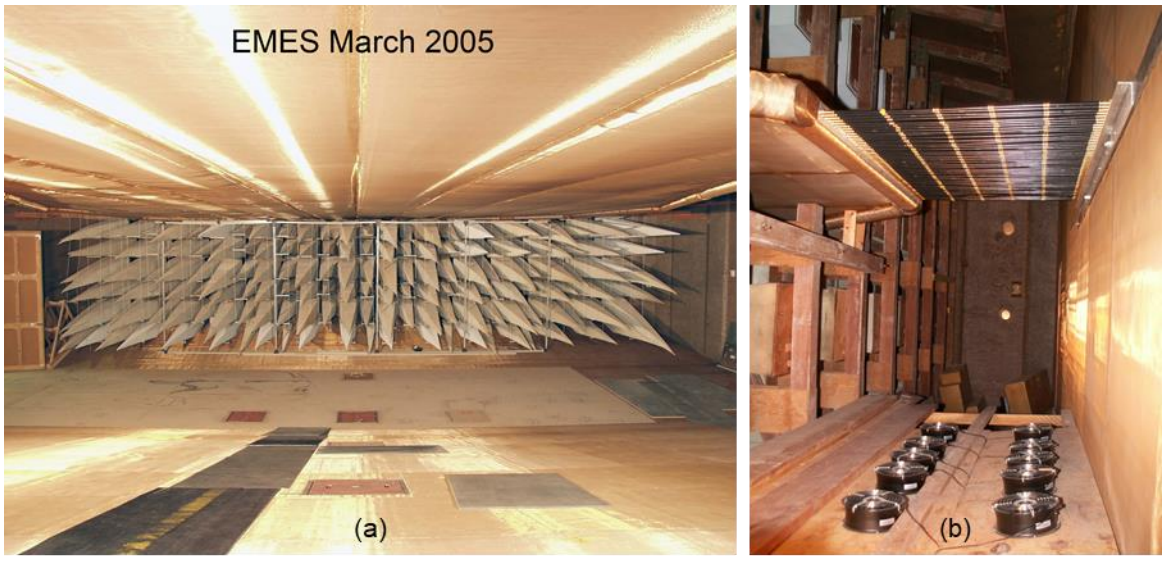

Figure 2-2. (a) EMES working volume in 2005 with a non-metallic support structure to mitigate RF absorber degradation and (b) parallel resistor assembly behind the RF absorbers.

Test articles are typically centered under the septum in the working volume, which also serves as the origin point for characterizing the field environment. A patch panel along the wall separating the EMES control room from the working volume enables sensor interfaces inside a test article to connect to measurement instrumentation in the control room. Fiber optic transmitter systems are used to maintain signal integrity and to mitigate electromagnetic coupling to instrumentation cables from the fields in the working volume. The test article response to different plane wave incidence angles and field polarizations at EMES is determined from additional experiments with different test article orientations. A diagram of the EMES pulsed mode and signaling sequence is illustrated in Figure 2-3.

The EMES facility is primarily used for high-altitude EMP testing and low frequency RF plane wave testing. High frequency CW tests are not typically performed at EMES due to the existence of cavity modes. Some EMES performance characteristics are shown in Table 2-1, and the working volume dimensions are shown in Figure 2-4. EMES can support electric field rise times less than 1 ns and a wide range of pulse amplitudes ranging from 25 kV/m to 250 kV/m when fed with a high fidelity pulser [2]. The resulting pulse has a similar shape to the IEC 61000-2-9 standard definition for the E1 radiated environment, with a 10-90% rise time of 2.4 ns (equivalent to IEC) and a full-width half-maximum of around 37 ns (roughly 50% wider than IEC). Normalized plots of an example measured EMES field pulse and the IEC waveform for early-time HEMP (E1) are shown in Figure 2-5.

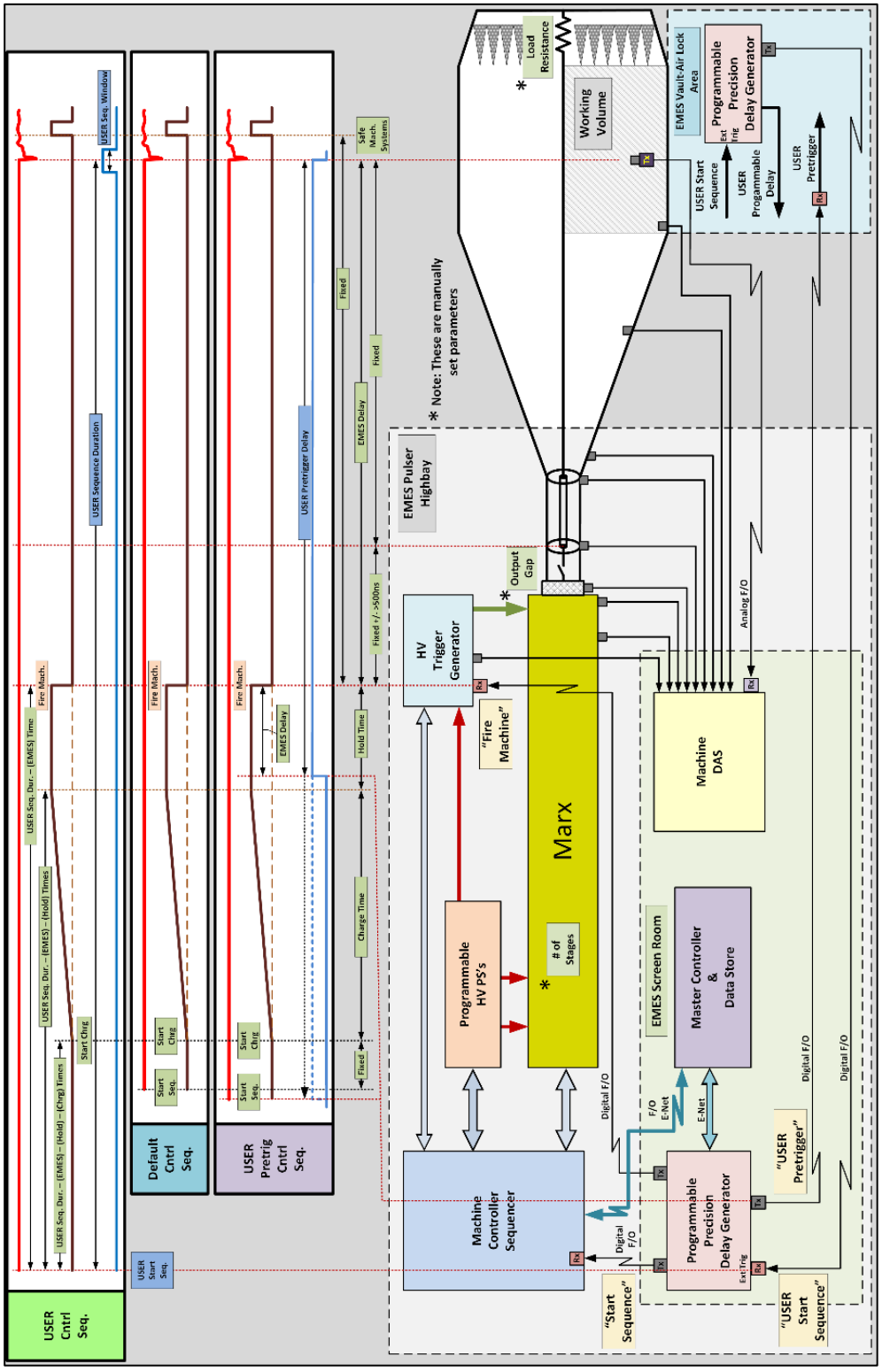

Figure 2-3. EMES Setup for Pulsed Testing and Signal Block Diagram.

Table 2-1. Performance Characteristics of EMES

Characteristic Description	Characteristic Value
Working volume dimensions	4 x 11 x 5 m (H x W x L)
E-field polarization	Vertical
Electric field intensity (max)	
• CW (0.010 – 0.100 MHz)	35 V/m @ 4 m septum height
• CW (0.100 – 250 MHz)	125 V/m @ 4 m septum height
• Pulsed	250 kV/m @ 4 m septum height
Pulse rise time (min)	≈1 ns

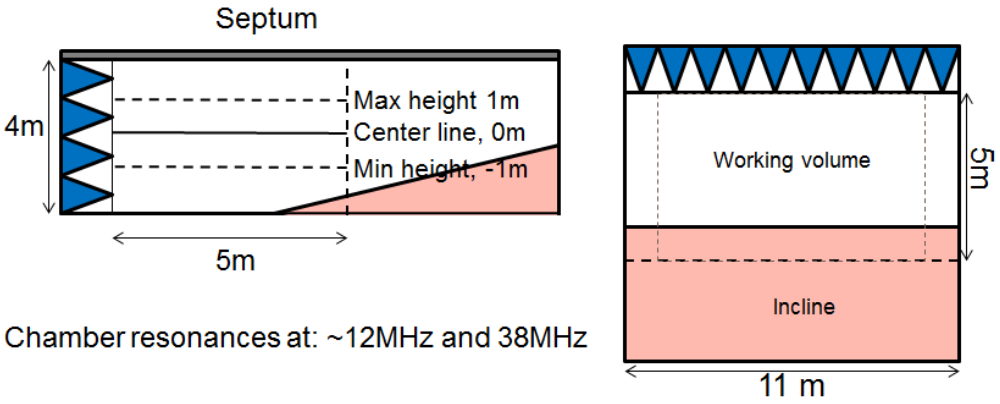

Figure 2-4. EMES working volume dimensions.

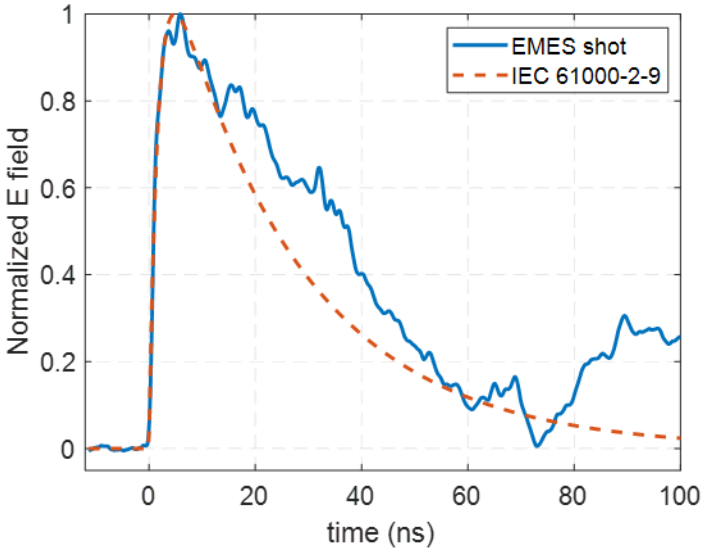

Figure 2-5. Normalized example field measurement from EMES compared to the normalized standard IEC waveform for E1.

2.3. Test Configuration

2.3.1. Test Setup

For this series of tests, the PV modules (5'5" W × 3'3" H) were mounted on a foam block (5' W × 4' H × 3' D) using wooden slats and oriented to face the chamber feed section. This orientation was believed to represent a maximum coupling configuration, where conductor traces connected to the outputs of the module are directly aligned with the incident field. The module was terminated in a 4.6 Ω load to represent a load connecting the module to a larger power grid. The load was enclosed in a metal box so additional coupling would not occur directly to exposed load connections.

During some of the E1 tests, the modules were illuminated by an LED light source as shown in Figure 2-6. The intent was to compare tests with and without the LED light source to see whether illumination is a factor for damage or coupled current. Unfortunately, it was not feasible to subject the module to standard test condition lighting (1 kW/m^2) within the EMES chamber. The LED source available for this environment provided only a very low level of relatively nonuniform illumination. The test setup can be seen in Figure 2-6.

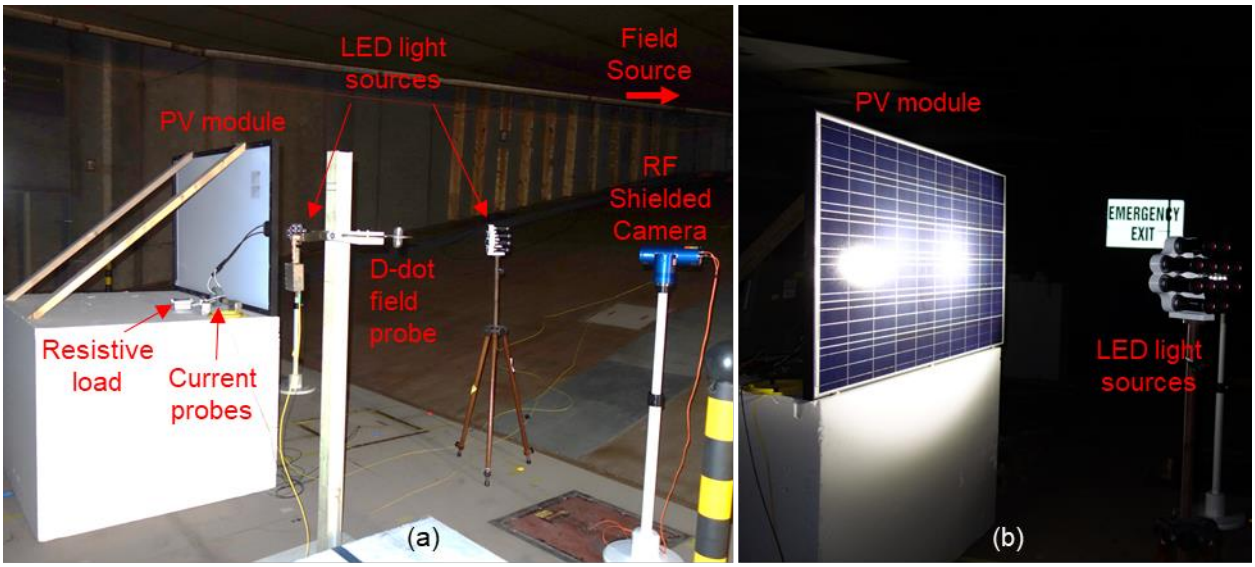

Figure 2-6. EMES test setup (a) during assembly, and (b) illuminated for test.

2.3.2. Test Unit Description

All modules tested were ET Solar ET-P660260WB multicrystalline silicon monofacial front-contact solar modules with the following manufacturer specifications at standard test conditions:

- Peak Power: 260 W
- Module Efficiency: 15.98%
- Open Circuit Voltage (Voc): 38.09 V
- Short Circuit Current (Isc): 8.84 A
- Rated Voltage (Vmpp) 31.48V
- Rated Current (Impp) 8.26A
- Power Tolerance +/- 3%
- Maximum System Voltage: 1000 VDC

- Nominal Operating Cell Temperature 45.3+/-2C
- Series Fuse Rating 15 A
- Number of bypass diodes 3

Nine modules were obtained for testing and were sequentially numbered based on the order that their state of health was first tested (henceforth referred to as modules 1-9). There was no physical difference between the modules otherwise. During experimental measurements, all modules were terminated with a 4.6 Ω resistive load. The resistance that would have placed the PV module at its maximum power point under standard test conditions was approximately 3.8 Ω, and the 4.6 Ω resistor used was the closest-available value.

Module 3 was set aside as a designated experimental control for comparing the state of health of the other modules qualitatively. Module 3 was not exposed to the TEM cell or insulted in any way aside from regular state of health checks consisting of I-V curve measurements under natural sunlight. This allowed a direct comparison of the state of health between the modules being tested and an untested module across multiple tests. This point of comparison is usable independent of local irradiance data or other external conditions.

2.3.3. Test Instrumentation

2.3.3.1. Experimental measurements

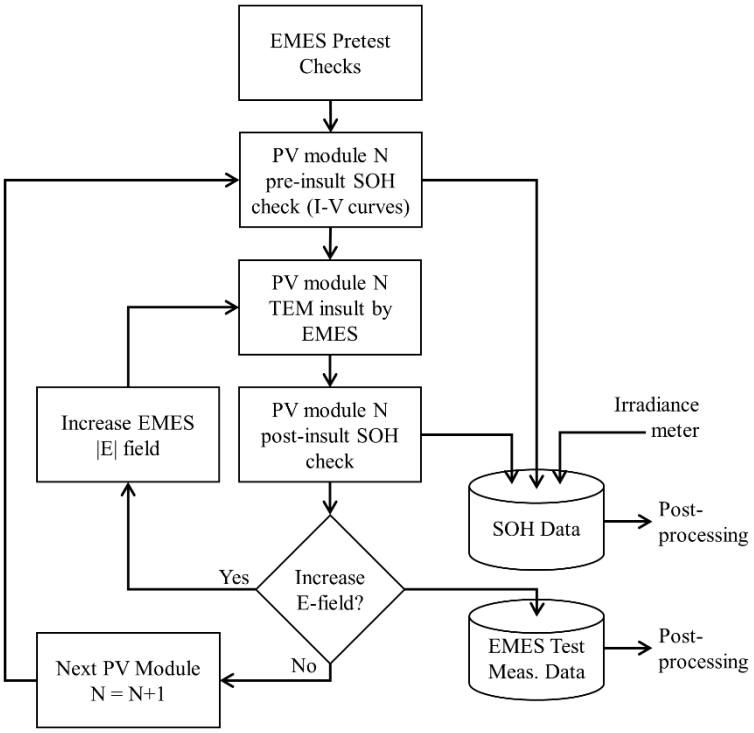

Figure 2-7. Experimental flowchart

The primary experimental process is defined in Figure 2-7. Following initial EMES field characterization, the state of health (SOH) was checked for both sample and reference modules. The sample module was then subjected to an EMES pulse and the state of health was measured again.

This process was repeated for each peak field value being tested. Each state of health check generated I-V curve traces, and the sample module metrics of short circuit current and peak power were checked against the reference module for general agreement before the next shot.

EMES pulse data was recorded using a Prodyn AD-40 electric field (D-Dot) sensor connected to BIB-100D Balun that measures the derivative of the electric field. The D-Dot had a 3dB cutoff above 1 GHz and risetime resolution of less than 1 ns. The balun had a 3dB bandwidth of 22 kHz-1.4 GHz. This sensor was mounted inside the EMES test chamber at the corner of the working volume during testing. The probe output was processed to find the electric field pulse levels. Coupled currents on the PV module from the E-field were measured using current transformers (CTs) clamped around the output cables going to the representative load. A Prodyn I-125-1HF probe was used for the common mode current and a Fischer F-70 was used for the differential mode current, as can be seen in Figure 2-8. The CTs were measured to have a primarily resistive response up to 100 MHz. All three probes were connected to broadband oscilloscopes in the EMES control room via fiberoptic links.

In addition to the test metering, an RF shielded CCTV camera was mounted in the EMES working volume to obtain a video recording of the tests. The camera was installed with motor control cables removed and cable connector apertures shielded to prevent interference from the chamber signal.

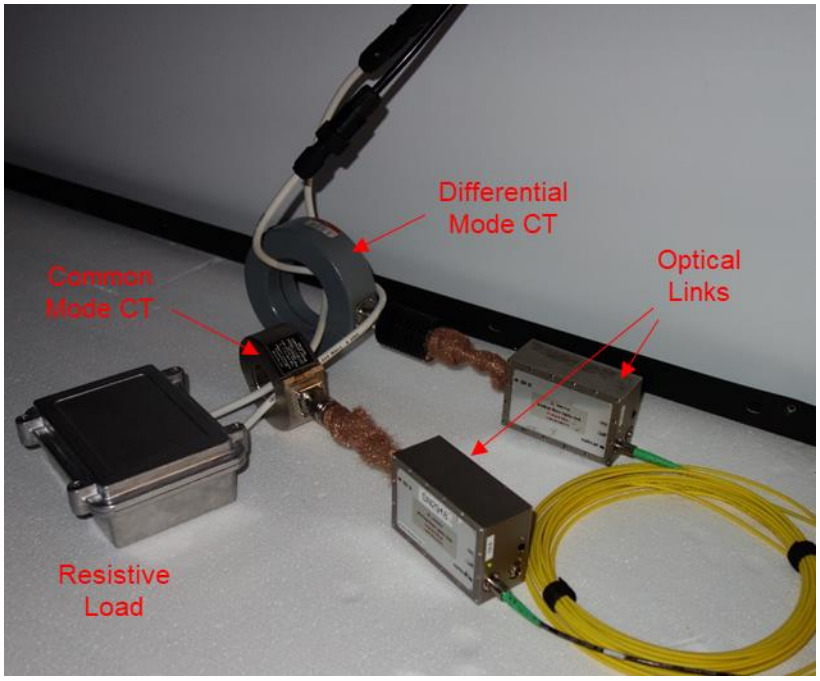

Figure 2-8. CTs for current measurement.

2.3.3.2. State of health

State of health for the PV modules to determine damage or loss of function was performed using I-V curve trace measurements. A Daystar Photovoltaic I-V Curve Tracer was used to measure the current and voltage through a swept variable resistance. The typical I-V curve values used to assess PV module health are the open circuit voltage, short circuit current, fill factor, and peak power. Damage to a PV module would be indicated by a significant shift in one of these properties that was not corroborated by a shift in the module 3 I-V curve taken as reference (i.e. a shift not coinciding with the conditions under which the sweep was performed). Sweeps were conducted before the first

shot on each module and after each EMES insult. State of health was measured outside of EMES with the 99 cm tall module leaning against the south-facing wall of the building at a marked point 91 cm from the ground, giving a calculated angle of 66.8°. The module orientation for this measurement is shown in Figure 2-9. Modules' I-V curves were compared against the control device (module 3), and peak measured power was compared to irradiance data measured during the same time window. Visual inspection of modules was also performed to determine any observable damage or alterations.

Figure 2-9. Module setup on exterior wall for I-V curve trace measurements.

Each I-V curve result can be normalized against the solar irradiance, module tilt, and module orientation occurring at the same time as the I-V trace measurement. This ideally removes the effects of variation in solar irradiance that arises from measuring the I-V curves outside. The curve normalization follows the process shown in Figure 2-10 and Equation (1).

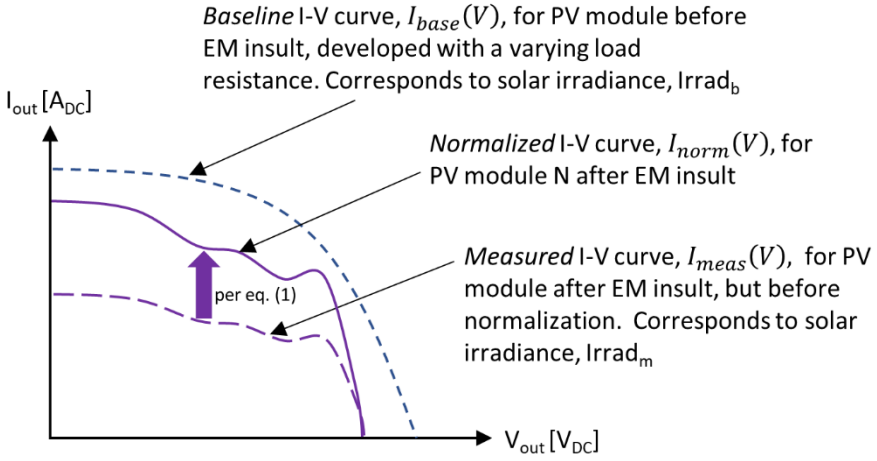

Figure 2-10. Description I-V curve normalization with respect to irradiance.

$$I_{norm}(A) = \frac{Irrad_m}{Irrad_b} I_{meas}(A) \quad (1)$$

The process for normalization was based on the use of direct normal and diffuse horizontal irradiance data that was obtained from solar instruments located about 0.25 miles away from the I-V curve trace location. The distance between the I-V curve trace location and the location of the irradiance meters allowed for the possibility of cloud shadows to bias information, but very few clouds existed during testing. As a precaution, the module 3 measurements were used as a backup means of normalization. The reference module was mounted in the same position as the sample modules and measured within minutes of each other. Measured output data for this reference PV module next to the sample measurements are shown in Table A-1. Comparisons between all measured I-V curves are shown in Appendix B.

The fill factor for a PV module is a scalar state-of-health metric that relates to factors such as the modules' series and shunt resistances and its reverse saturation current [2], and changes in the fill factor would be indicative of shifts in these module parameters. This makes the fill factor a good state-of-health metric for present purposes. Fill factor is defined as a ratio of the PV module's maximum power and its short circuit power, as shown in Equation (2).

$$FF = \frac{I_{mp}V_{mp}}{I_{sc}V_{oc}} \quad (2)$$

Where mp represents the maximum power point on the I-V curve trace, I_{sc} is the short-circuit current, and V_{oc} is the open-circuit voltage. Fill factor is used to represent the approximate useful capability of a PV module as a percentage of its theoretical maximum. This ratio is shown in Figure 2-11. Within this work all fill factor calculations used normalized current based on the measured irradiance data as defined in equation (1). Data normalization is not expected to change the value calculated in equation (2) due to both short circuit current and peak power current being normalized by the same irradiance values but is performed as the standardized approach to this calculation.

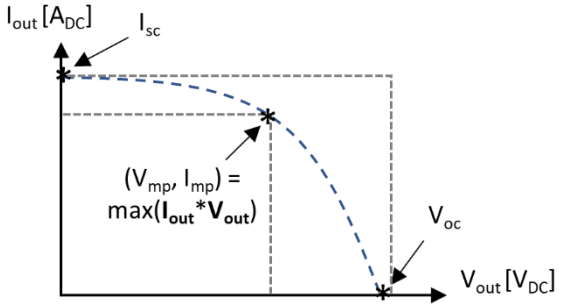

Figure 2-11. Description of the Fill Factor metric on a normalized PV module I-V curve.

Following the test sequence and state of health measurements discussed in this report, additional state of health analysis was performed at Sandia's Photovoltaic Systems Evaluation Laboratory (PSEL) using flash I-V curve measurements and electroluminescence imaging. The outcomes of these procedures are discussed in Appendix C.

2.4. Test Procedures

2.4.1. Test Matrix

Module testing followed the sequence detailed in Table 2-2. Target field values were defined as the approximate E-field peak that the EMES pulser settings were meant to achieve. Due to variability in pulser performance, any peak within 10-15% of the target is considered adequate. The measured

field values during testing are discussed in detail in Section 3, and the full shot log is recorded in Table A-1 of Appendix A.

Table 2-2. Test Matrix

Module #	Target Field Values for each Shot
1	• 25 kV/m (dark and illuminated) • 35 kV/m (dark) • 50 kV/m (dark and illuminated) • 65 kV/m (dark) • 80 kV/m (dark) • 100 kV/m (dark and illuminated)
2, 4-7	• 60 kV/m (dark) • 80 kV/m (dark) • 100 kV/m (dark)
8	• 60 kV/m (dark) • 80 kV/m (dark) • 100 kV/m (illuminated)
9	• 60 kV/m (dark, vertical and planar orientations) • 80 kV/m (dark, vertical and planar orientations) • 100 kV/m (illuminated, vertical and planar orientations)

Prior to testing, each module underwent baseline state of health testing using the I-V curve tracer. Module 3 was measured either immediately before or immediately after to serve as a reference. The state of health check was performed again after each shot, with module 3 again measured immediately before or after. Module 3 was never exposed to the EMES field and was only used for state of health comparisons to other modules. After state of health testing the module under test was returned to the working volume for the next shot.

Module 1 testing was used to calibrate the attenuation and scope settings for the probes and therefore contained more discrete E-field values for shots and sometimes more than one shot at each field value. State of health was checked, at a minimum, for the first and last shot at each field level to confirm initial survivability at each new field level and PV module function prior to the next field level test. The original intent was to reach 50 kV/m during testing per the IEC standard for the peak radiated E1 field [1]. However, no reduction in state of health was observed at this field level for module 1 as compared to module 3, so higher field levels were tested for the remaining modules.

The number of stages in the EMES pulser source had to be reconfigured for target field values greater than 50 kV/m, so all shots starting with module 2 began at 60 kV/m and scaled up to 100 kV/m. Likewise the presence of LED illumination was not found to significantly alter the response or the state of health of module 1 while testing, so additional illuminated shots were reserved for high voltage levels only to obtain video from the RF shielded camera.

Module 9 was tested using a vertical orientation with the longer axis of the module in parallel with the field (see Fig Figure 2-12a) or a planar orientation with the module face parallel to the overhead septum (see Figure 2-12b). In this way, the full range of potential angles between the direction of travel of the TEM wave and the surface of the module was investigated.

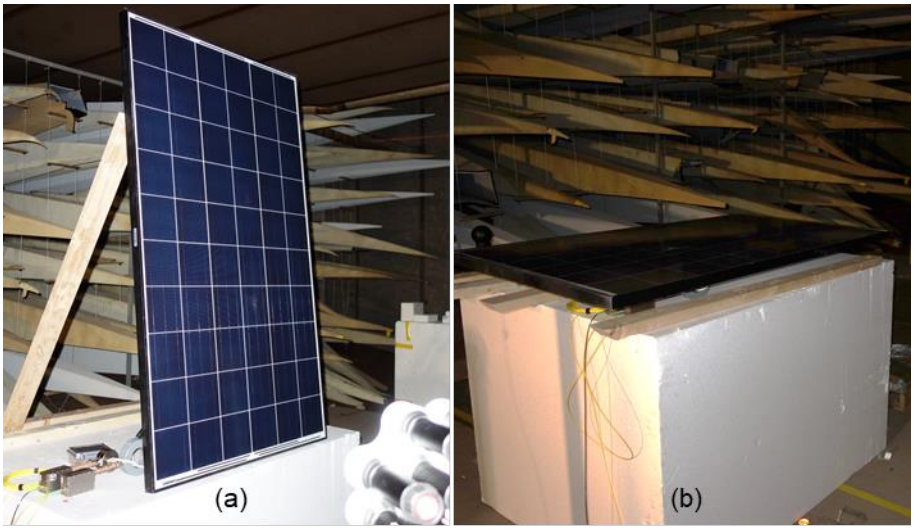

Figure 2-12. Alternate setups for module 9 testing in (a) vertical orientation and (b) planar orientation.

2.4.2. Test Steps

The formal test steps are detailed below:

1. Prior to placing device under test in the working volume
   a. Perform environmental characterization of chamber
      i. Place Prodyn AD-40 electric field (D-Dot) sensor and BIB-100D balun in center of working volume
      ii. Ensure D-Dot is connected to fiberoptic link
      iii. Conduct pulsed test of empty chamber at 25 kV/m
         1. Please reference TWD "Department 1353 FREMP_TWD_Rev E" [3] for proper EMES operating procedure guidelines
      iv. Post pulsed test
         1. Ensure test is complete and chamber is safe to enter
      v. Repeat steps 1.a.i-1.a.iv for D-Dot at second and third positions for characterization
      vi. Repeat steps 1.a.i-1.a.v for field strengths of 35 kV/m and 50 kV/m (or desired field strengths)
      vii. Place D-Dot in field measurement position on the side of the working volume.
2. Prior to conducting pulsed test
   a. Perform I-V trace state of health measurement on device under test
      i. Lean PV module on south-facing exterior wall of building at designated mark (91 cm high on South facing wall).
      ii. Connect I-V Curve Tracer to building power
      iii. Plug curve tracer into 9 pin serial port on back of laptop
      iv. Turn disconnect to Off, Range =1 (low)
      v. Connect PV sense, positive, and negative to curve tracer
      vi. Connect positive and negative to PV module
      vii. Plug in curve tracer and turn on

viii. Open IVPC3 program on computer (desktop icon)
ix. Settings > Communication port
x. Ensure that tracer is visible on COM1
xi. Turn disconnect to ON
xii. Click New Curve icon
xiii. Once tracer is charged, click Take Curve
1. NOTE: necessary current and voltage levels for test should be automatically determined by IVPC3 program
xiv. View > Datapoints
xv. Click Select All
xvi. Select Copy
xvii. Open excel and paste data
xviii. Save data
xix. Record initial values of open circuit voltage, short circuit current, and maximum power (and corresponding voltage and current)

b. Disconnect I-V curve tracer from PV module
c. Repeat Step 2a on experimental control (Module 3)
i. NOTE: Module 3 can be measured first, in which case the device under test is measured in this step.

3. Conducting pulsed test
a. Mount PV module on top of foam block with wooden legs
b. Place LED light sources in appropriate position to the module
c. Attach representative load to output cables from PV module
d. Connect CTs and protective circuit to output cable of PV module and ensure that CTs are connected to fiberoptic link
i. Unless otherwise noted, connect Fischer CT in differential mode and Prodyn CT in common mode.
e. Ensure D-Dot is connected to fiberoptic link
f. Set up TDK camera
i. Position camera to ensure view of LED light sources and PV module
ii. Remove motor control cable
iii. Cover cable connector apertures with copper tape
g. For illuminated tests in the test matrix, turn on LED light source
h. Ensure all personnel are out of working volume and close chamber for testing
4. During pulsed testing
a. Please reference TWD "Department 1353 FREMP_TWD_Rev E" [3] for proper EMES operating procedure guidelines
5. Post pulsed test
a. Ensure test is complete and chamber is safe to enter
b. For illuminated tests in the test matrix, turn off LED light source
c. Repeat steps 2(a)-2(c) to perform state of health check on PV module under test and experimental control

i. Evaluate short circuit current, open circuit voltage, and maximum power compared to initial values.
    1. If substantial damage is detected (substantial shift in above values not reflected in experimental control), the PV is considered to have failed and the test matrix is stopped.
    2. If minor change is detected (acceptable shift in above values or substantial shift reflected in experimental control), the next voltage level is tested to a maximum of 100 kV/m.

d. For module 1 only, evaluate CT measurements to determine whether attenuation is appropriate, whether saturation of CTs and optics can be identified, and adjust setup accordingly. Repeat pulsed test as needed.

6. Repeat steps 2-5 for next module in test matrix.
7. For any shots needed to characterize the environment, continue to obtain CT and D-dot data to serve as noise measurements.
8. Perform additional noise measurement for 100 kV/m shot with a PV module present (module 9) but disconnected from load once all testing has been concluded.

2.5. Post-processing

Following each shot, the derivative electric field measured by the D-dot probe was integrated using the following steps:

1. Window the data to 12 ns before and 1 μs after the measured minimum (greatest change in field or the rise time of the pulse).
2. Filter the pulse data between 0.2 and 1000 MHz.
3. Subtract the average of the windowed data to remove any DC offset.
4. Detrend and integrate data.
5. Multiply by any attenuation factor based on the experimental setup.
6. Convert the integrated scope voltage to electric field using the equation $E = \int V_0\, dt/\varepsilon_0 R A_{eq}$, where V_0 is the measured voltage, $\varepsilon_0 = 8.85 \times 10^{-12}\ F/m$ is the free-space permittivity, $R = 50\ \Omega$ is the input impedance of the probe, and $A_{eq} = 0.01\ m^2$ is the equivalent area of the probe.
7. Set the beginning of the pulse to 0 time and subtract the average of the noise data prior to the pulse to level the beginning of the pulse to zero.

The filtering in step 2 was applied to remove any DC effects and high frequency scope noise from the resulting measurements. For the field measurements in this report, the signal-to-noise of the D-Dot probe data was high enough to not need significant filtering, while the DC effects were handled by average subtraction and detrending. For this work, detrending was done via a MATLAB function which identifies and removes linear behavior across the measured field vector. The attenuation factor was defined by the coaxial attenuators attached to the balun prior to the optical link to prevent saturation of the optical link or scope. For this series of measurements, the D-Dot attenuation was a linear factor of 2244.

The difference between the data just before the event and the absolute maximum calculated field is then defined as the peak field reached. Since EMES performs best as a delivery system for electron charge (negative potential on the septum with respect to ground), the resulting field measurement appears as a negative pulse, with the electric field peak taken from the minimum of the pulse. EMES

allows anywhere from a 10-15% accuracy margin in peak field value when targeting a specific maximum.

The coupled current from the field into the PV module was calculated by multiplying the measured voltage from each CT at the scope by the attenuation factor and then dividing by the impedance of each CT probe. However, since the EMES shot has a broadband spectrum, the measured frequency-dependent impedance is used instead of the single value resistance that defines the operating range of the probes. The measured transfer impedances are shown in Figure 2-13, which can be compared to the manufacturer transfer impedance values of 5 Ω for the Prodyn probe and 1 Ω for the Fischer probe. For both cases the probes are at rated values up to roughly 100 MHz. The Fischer CT is consistent below 200 kHz, while the Prodyn CT begins to drop off below 1 MHz. The first frequency step after DC is 200 kHz in the Fourier transform of the measured scope data, so any trends below this limit are not considered.

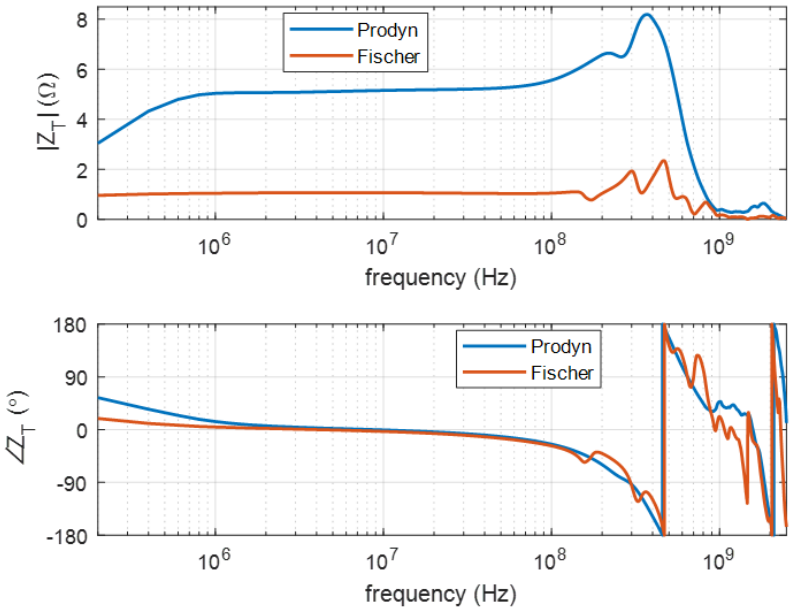

Figure 2-13. Transfer impedance (a) magnitude and (b) phase with respect to frequency for Prodyn and Fischer CTs.

3. TEST RESULTS

3.1. Shot Data and Failure Testing

3.1.1. Module 1

Testing on module 1 was used to define the field levels used for later modules and to calibrate CT measurements. The field levels for module 1 were increased to the next target once the module was confirmed to survive via SOH and no large measurement setup concerns were observed, even if the CT attenuation and scope settings were still being calibrated. The shots are cataloged in Table 3-1.

Table 3-1. Module 1 Shot Data

Date	Shot #[1]	EMES Field Target[2] (kV/m)	EMES Actual Field (kV/m)	Illumination[3]	Notes
10/10	7	25	23.9	Dark	LEDs used for SOH, invalid I-V curve.
10/10	8	25	23.1	Dark	LEDs used for SOH, invalid I-V curve.
10/10	9	25	25.1	Dark	LEDs used for SOH, invalid I-V curve.
10/14	1	25	27.8	Dark	CT calibration. SOH stable, no ref[4].
10/14	2	25	27.5	Illuminated	CT calibration. SOH stable, no ref[4].
10/14	3	25	27.5	Dark	CT comparison. SOH skipped.
10/14	4	25	28.3	Dark	CT scope calibration. Good SOH vs ref[4].
10/14	5	35	37.5	Dark	CT scope calibration. SOH stable, no ref[4].
10/14	6	35	35.6	Dark	CT comparison. SOH stable, no ref[4].
10/14	7	50	45.7	Dark	CT calibration. Good SOH vs ref[4].
10/14	8	50	44.8	Illuminated	CT check. Good SOH vs ref[4].
10/15	6	50	45.9	Dark	Increased pulser stages. Good SOH vs ref[4].
10/15	7	65	61.4	Dark	CT scope calibration. SOH stable, no ref[4].
10/15	8	65	56.4	Dark	Low peak, shot repeated. SOH skipped.
10/15	9	65	58.2	Dark	Low peak, shot repeated. SOH stable, no ref[4].
10/15	10	65	67.2	Dark	Good shot and CT data. Good SOH vs ref[4].
10/15	11	80	81.6	Dark	Good shot and CT data. Good SOH vs ref[4].
10/15	12	100	117.8	Dark	Good shot and CT data. Good SOH vs ref[4].
10/15	13	100	125.0	Illuminated	Good shot and CT data. Good SOH vs ref[4].

[1] Shot # refers to the sequential number of shots for a given date. Shots 1-6 on 10/10 and shots 1-5 on 10/15 were used for test chamber field measurements when no sample was present and are not part of the test sequence. Information for these shots is in Appendix A.

[2] The target field is the peak electric field value that was intended by the EMES pulser settings based on past electric field measurements. EMES allows a 10-15% variation between the target field and actual field peak.

[3] Illumination refers to whether the LED arrays directed at the module were illuminated or dark. Illumination was used for visualization only and had no observable effect on module response.

[4] The reference I-V curves were taken from Module 3, which had no EMES exposure, for comparison against the sample.

The first day of testing used LEDs for illumination for I-V curve tracer measurements, which were deemed to be insufficient for proper PV module response. Additional details are given in Appendix B. For the second and third days of testing, module 1 state of health was tracked while calibrating attenuation and scope settings for the CT measurements. The second set of tests stepped from 25 kV/m to 50 kV/m. The final shot at each voltage level is shown in Figure 3-1a as a subsampling of data for the three E-field values tested. Figure 3-1b corresponds to each shot represented in Figure 3-1a in addition to the blue curve indicating the initial state of health prior to any EMES insults. The system was then reconfigured for the third set of tests which stepped from 50 kV/m to 100 kV/m. The final shot at each voltage level is shown in Figure 3-1c. The corresponding state of health curves are shown in Figure 3-1d, once again with the blue curve indicating the measurement taken prior to the series of tests.

Some variation is observed among the state of health shots for module 1 that correspond roughly to the time of day that the sweeps were taken. This is particularly noticeable in Figure 3-1d for the sweeps taken for original state of health and after the 50 kV/m and 100 kV/m shots. More direct analysis of the status of module 1 was obtained with comparison to module 3 measured during the same time frame. Table 3-2 details the peak output power from the I-V curves of module 1 and module 3 associated with the shots in Table 3-1. In general, the peak power of module 1 measured within 10% of module 3 except for shot #6 on 10/15. This is likely due to a shift in external lighting conditions at the time of measurement that caused the variation, since measurements taken after the fact show continued agreement between the two modules with no clear trend of degradation. Additional nonlinear variations in the current profile below the peak power observed at the knee are characteristic of variable lighting conditions as well and were consistent between the sample and reference measurements. The individual I-V curves are plotted in Appendix B. Module 1 was shown to survive an E1-like pulse with field values up to 125 kV/m measured peak with no apparent loss of module functionality and no physical damage. Consistent positioning and orientation of the sample and reference using the exterior wall of the facility was incorporated starting with shot #6 on 10/15 and corresponds to the beginning of the associated irradiance data collection, which is addressed in Section 3.1.2.3.

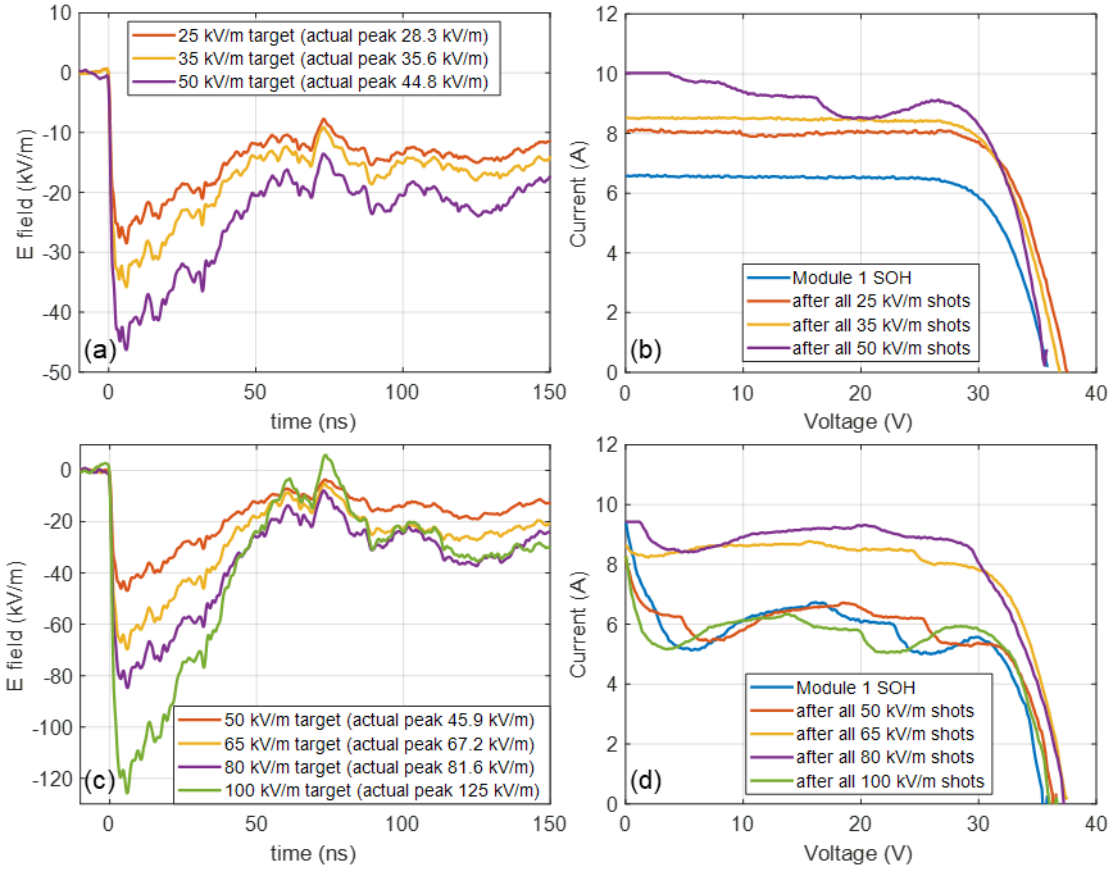

Figure 3-1. Module 1 shot response for (a) measured E-field pulses on 10/14 and (b) resulting state of health and for (c) measured E-field pulses on 10/15 and (d) resulting state of health.

Table 3-2. Module 1 State of Health Tracking

Date	Shot #	Target Field (kV/m)	Actual Field (kV/m)	Module 1 Peak Power (Sample, W)	Module 3 Peak Power (Reference, W)	Peak Power Ratio of Sample to Control
10/14	SOH	-	-	179.0	194.4	0.92
10/14	4	25	28.3	231.9	228.1	1.02
10/14	7	50	45.7	236.5	225.3	1.05
10/14	8	50	44.8	253.1	250.7	1.01
10/15	SOH	-	-	167.3	178.8	0.94
10/15	6	50	45.9	166.9	194.9	0.86
10/15	10	65	67.2	237.7	215.2	1.10
10/15	11	80	81.6	250.3	252.6	0.99
10/15	12	100	117.8	208.0	199.6	1.04
10/15	13	100	125.0	167.8	161.5	1.04

3.1.2. Additional Module Measurements

Measurements of additional samples following module 1 were reduced to three settings of the EMES pulser with target electric field levels of 60 kV/m, 80 kV/m, and 100 kV/m. A sampling of the actual measured electric field for the three settings is shown in Figure 3-2 for the module 2 tests. For the three settings, the actual measured electric field peaks were 64.8 kV/m, 77.4 kV/m, and 106.3 kV/m, all within reasonable accuracy of the EMES settings. Actual peak values of all shots across all modules are given in **Error! Reference source not found.** in Table A-1.

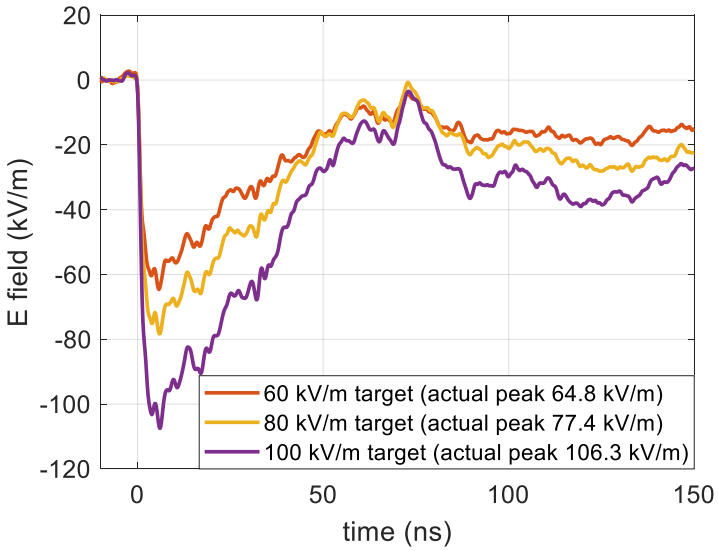

Figure 3-2. Representative shot data from module 2 for 60 kV/m, 80 kV/m, and 100 kV/m target electric field values.

The state of health of each module from 2 to 9, excluding module 3 which was used as the reference, was measured prior to any shots on the module and after each shot. Module 3 power measurements (V*I) were taken immediately before or after the module under test. This ensured that consistent solar irradiance tracking and PV module baseline data were collected for each tested device. While each I-V curve taken for the modules under test was associated to a measured solar irradiance value, the use of Module 3 provided a second means of baseline data independent of external conditions. Samples of the I-V curve traces taken across single-module testing are shown in Figure 3-3 for modules 2, 4, 5, and 6. It should be noted that the SOH measurement for module 2 in Figure 3-3a shows low overall current and oscillatory behavior, which indicates partial shading at the time of measurement. This was most likely due to cloud cover and similar behavior was observed for module 3 taken at the same time. Modules 4, 5, and 6 in Figure 3-3b-d show much more consistent behavior across the test series. There is no indication of an overall diminished behavior in the modules from the observed state of health data, just variation from measurement to measurement that can be compared to the reference measurement taken at the same time. Full comparisons of all I-V curves taken for each sample, as well as the associated module 3 reference measurements, are given in Appendix B. More rigorous state of health checks performed after all testing are detailed in **Error! Reference source not found.**.

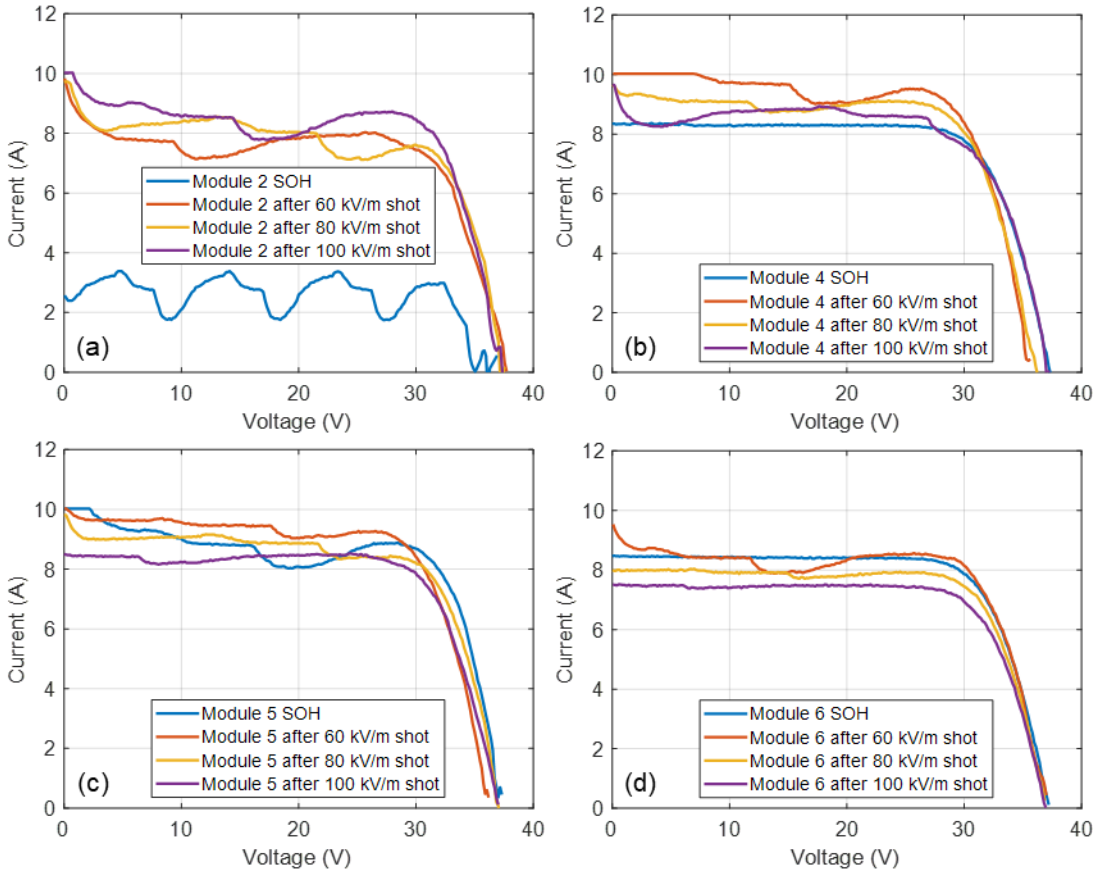

Figure 3-3. Sampling of state of health tracking for individual modules after each shot for (a) module 2, (b) module 4, (c) module 5, and (d) module 6 without normalization against irradiance. Accompanying measurements of reference module 3 and samples 7-9 are provided in Appendix B.

3.1.2.1. State of health correlated to trends in fill factor

For each PV module, the resulting values of fill factor were plotted on the same axes and fit to a polynomial, which included the calculation of standard error estimates. A Gaussian probability density function (PDF) was developed which would estimate the probability of fill factor conditional upon the magnitude of the EM insult |E|. The PDF was developed using the functional form of mean and standard deviation (assumed to equal standard error). The conditional expected value is described by (3), and the conditional standard deviation is described by (4). The standard error was used as a good estimate of the standard deviation since number of data points used to fit the polynomial was significantly larger than the number of degrees of freedom of the polynomial.

$$\mu(|\hat{E}|) = -2.8609\text{-}04|\hat{E}| + 7.3795e\text{-}01 \quad (3)$$

$$\sigma(|\hat{E}|) = -1.5024e\text{-}05|\hat{E}| + 8.2474e\text{-}02 \quad (4)$$

The Fill Factor conditional PDF is then given by (5).

$$P_{FF}(conditional\ on\ |\hat{E}|) = TND\left(\mu(|\hat{E}|), \sigma(|\hat{E}|)\right)\ [0\ 1] \quad (5)$$

where:

- TND – Truncated Normal Distribution (TND) Corresponding to $|\hat{E}|$ (truncated at 0 and 1)

- $\mu(|\hat{E}|)$ – Mean value of TND $|\hat{E}|$ per (3)
- $\sigma(|\hat{E}|)$ – Standard Deviation of TND at $|\hat{E}|$ per (4)
- $|\hat{E}|$ – Magnitude of the Electric Field During the HEMP Insult (scalar)
- $|E|$ – Magnitude of the Electric Field (continuous variable)

Equations (3-5) can be used to construct a TND for any given $|\hat{E}|$, which can then be sampled to estimate the post-insult fill factor for any PV module for use in Monte-Carlo or similar analyses. An example of this calculation being applied to data is shown in Figure 3-4. The prerequisite value of $|\hat{E}|$ can obtained via assumption, calculation, or measurement, as appropriate. Figure 3-5 is a graphical depiction of the TNDs as they describe the probability of PV module factor resulting from low $|\hat{E}|$ insult values (in blue) to high $|\hat{E}|$ insult values (in red). The x-axis of the graph extends from [0 1], although the PDFs were populated using data from [0 1]. Each PDF is defined per Figure 3-4, then truncated at [0 1] with unity area over this interval.

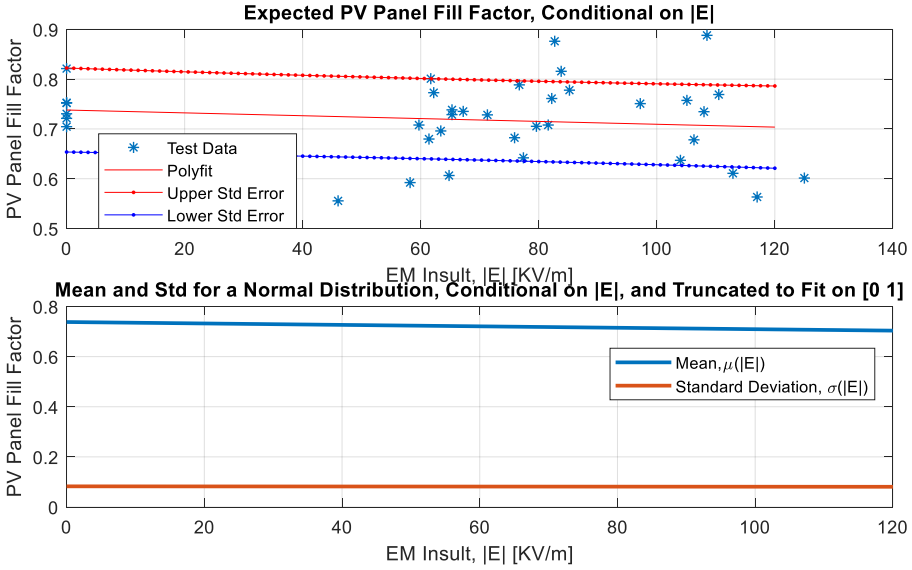

Figure 3-4. Definition of mean and standard derivation from calculated fill factor.

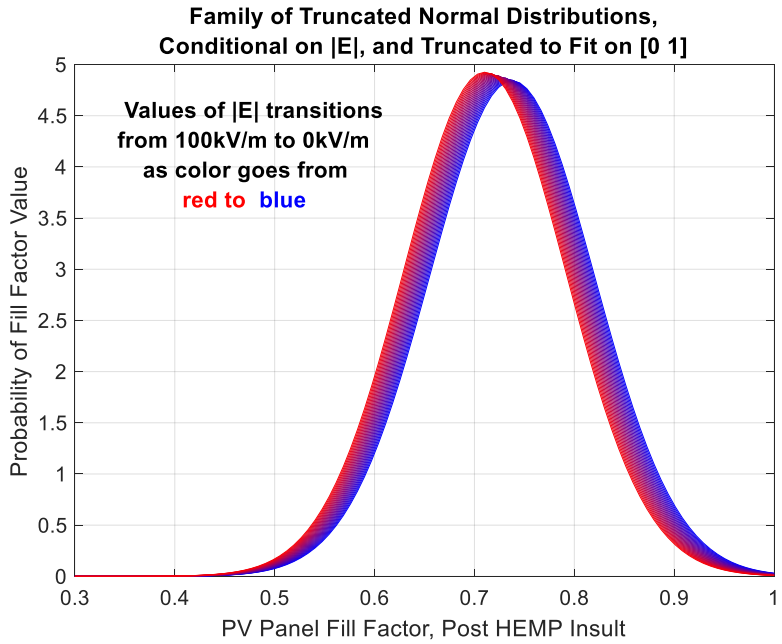

Figure 3-5. Use of Raw Test Data to Develop a Family of Conditional PDFs for FF(|E|)

From this data there is some suggestion of decrease in overall fill factor as the peak value of the HEMP insult increases. However, the overall observed trend for this data is small and the data points are widely distributed, which makes assertions of a trend difficult. Another way of looking at the fill factor is by tracking individual module response as shown in Figure 3-6. Here the fill factor calculations have been binned based on the target shot peak (initial state of health, 60 kV/m, 80 kV/m, and 100 kV/m) and the average of each is plotted with error bars representing the standard deviation. It should be noted that the state of health average neglects the first measurement point of Module 2, which exceeds the theoretical maximum fill factor value of 1. This erroneous value was due to poor measurement conditions at the time resulting in a curve with a lower short circuit current than the peak power current.

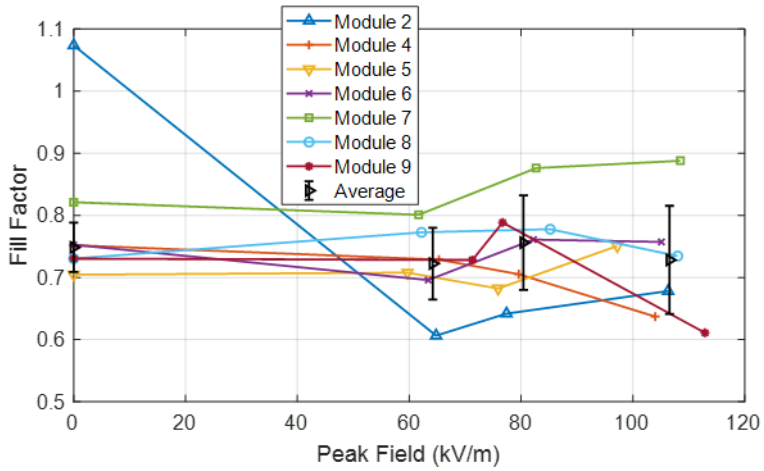

Figure 3-6. Fill factor tracking and averages for individual modules.

The results in Figure 3-6 show some variation in the average fill factor for each shot, though there is very little observable trend overall, with the final average fill factor falling only 3% from the initial

fill factor, which is within the initial standard deviation. The standard deviation of the fill factor does appear to increase as the EMES insult increases, but more data would be needed to determine whether these values are statistically correlated. There is not a strong enough observable trend within the different sets of state of health measurement to assert any overall degradation in PV module performance. At most, any observed degradation would be small rather than constituting a failure in the module, and this would only occur at fringe electric field levels (i.e. >50 kV/m) that are not anticipated in a realistic HEMP event.

3.1.2.2. State of health correlated to experimental control

One method of observing the state of health independent of variation due to time of day is by normalizing sample data against the reference module peak power, assuming that the measurements of module 3 and the module under test were taken reasonably close together. The peak measured power for each module across all state of health testing is normalized against the reference power and plotted in Figure 3-7. In all cases there is no obvious degradation observed for the modules by the end of testing. For modules 8 and 9 there is a significant dip in the power relative to the reference signal, and there is a drastic increase for modules 7, 8 and 9 following the final shot. These effects are likely due to irregular cloud cover on the day that these modules were measured, which caused significant variance between modules measured even minutes apart. In general, most of the sample modules measured a higher peak than the reference, which is most likely a due to the cleanliness of module 3, which spent more time outdoors than the other modules, rather than any indication of improved state of health. State of health checks were taken for module 9 after both vertical and planar orientations, but only the results after the planar shots are shown in Figure 3-7. Full details are given in Appendix A.

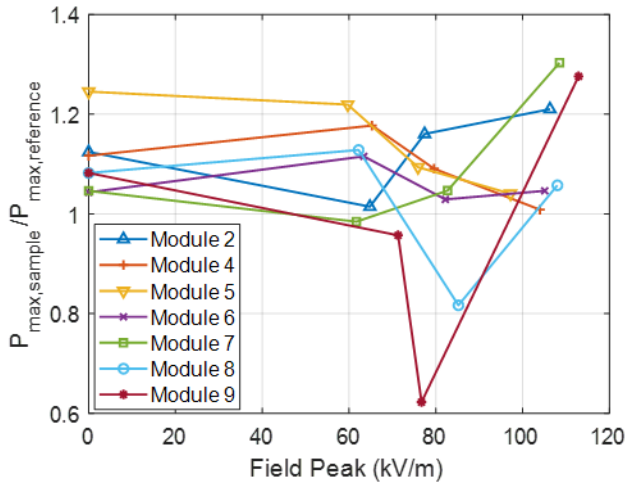

Figure 3-7. Normalized PV Power tracking for each module using peak power normalized against module 3. Trends indicative of state of health.

3.1.2.3. State of health correlated to local irradiance

Another way to observe the state of health trends for the modules is to compare against irradiance data, which should show the same trend regardless of time of day or cloud cover. Local irradiance data was obtained from continuous measurements collected on-site at Sandia roughly 0.25 miles from the site of the I-V curve tracing. The time stamps taken for the individual I-V curves denoting state of health were compared to local irradiance at the same time starting on 10/15 with the I-V curves following shot #6 on module 1, after which all state of health setups used the same

orientation. The full calculated irradiance data corresponding to the state of health checks is given in Appendix A in Table A-1. The trend of measured peak power vs irradiance is shown in Figure 3-8a for the sample modules and Figure 3-8b for the reference module 3. While some positive trend can be observed from this comparison, the points have a wide distribution even for the individual modules and therefore may not be useful for normalization the I-V curve data. The same degree of distribution is seen for the reference module measurements. This indicates that the discrepancy is most likely due to the distance and possibly a small difference in time between the I-V curve measurements and irradiance measurements. The I-V curve current (and subsequently the peak power) varies with module temperature as well, which was not tracked as part of this experiment and may have a greater effect on the peak than the irradiance alone. As a result, the irradiance data could not be fully utilized to correct for lighting conditions when evaluating state of health. Follow-up state of health metrics were performed using a more controlled light source instead and are detailed in **Error! Reference source not found.**.

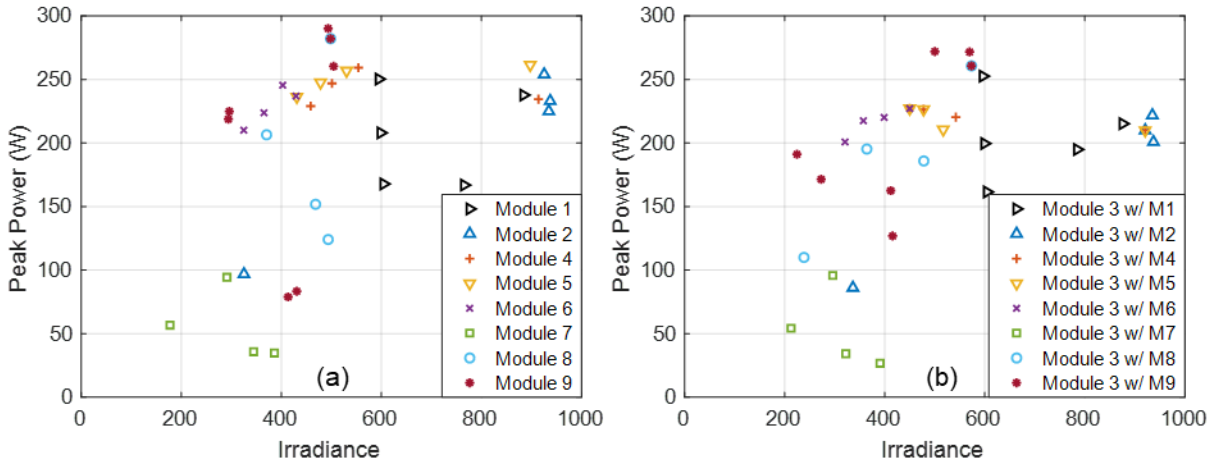

Figure 3-8. Measured peak power vs local irradiance for (a) all sample modules, and (b) module 3 serving as the reference.

3.2. PV Output During EMP Insult

In addition to state of health of the PV modules themselves, the coupled currents from the PV module to the load during HEMP are also of interest. While a radiated pulse may not damage the PV module directly, as determined by the state of health tracking above, the subsequent conducted pulse traveling from the PV module to a DC-DC converter or a DC-AC inverter may cause damage to that equipment. For the field exposure in this work, these pulses were measured using CTs on the output cables in common and differential mode to measure the current pulse. Common mode refers to the current traveling parallel or in the same along the signal and return connections of the PV module. Differential mode refers to the currents traveling around the loop of the PV module, connections, and load, and is measured as the difference between the two cable connections.

The differential and common mode currents measured from the modules during testing were consistent for each shot of the same strength and module orientation. Representative results for the horizontal orientation are given for module 8 in Figure 3-9., with measurements from the 60 kV/m shot in Figure 3-9.a-c, the 80 kV/m shot in Figure 3-9.d-f, and the 100 kV/m shot in Figure 3-9.g-i. The second and third plot for each voltage level is zoomed in to focus on the differential and common mode measurement of the current, respectively. In all cases the pulse is seen to generate a differential mode surge that is much slower than the incident field signal. This may be due to long

line lengths across the PV module or a slow response of the semiconductor material to the sudden field peak. Meanwhile the common mode current has a high frequency ringing that starts with a large peak and quickly dampens. For the experiment, the resistive load and module are not grounded, so the high frequency oscillations are most likely due to the cable length between the module and the resistive load causing multiple reflections at a specific frequency. In all cases the peak values of the two currents both increase proportionally to the field peak value, with the 100 kV/m shot generating a slow-moving -16.4–22.7 A signal in differential mode and an oscillating signal from -95.1–80.7 A in common mode. These coupled currents are of interest for modeling the expected coupling of the HEMP environment through the PV module into any connected DC-DC converter or DC-AC inverter. The conducted insult could be implemented experimentally using pulse generators or a damped sine source. Additional details on the current measurements are given in Table A-2.

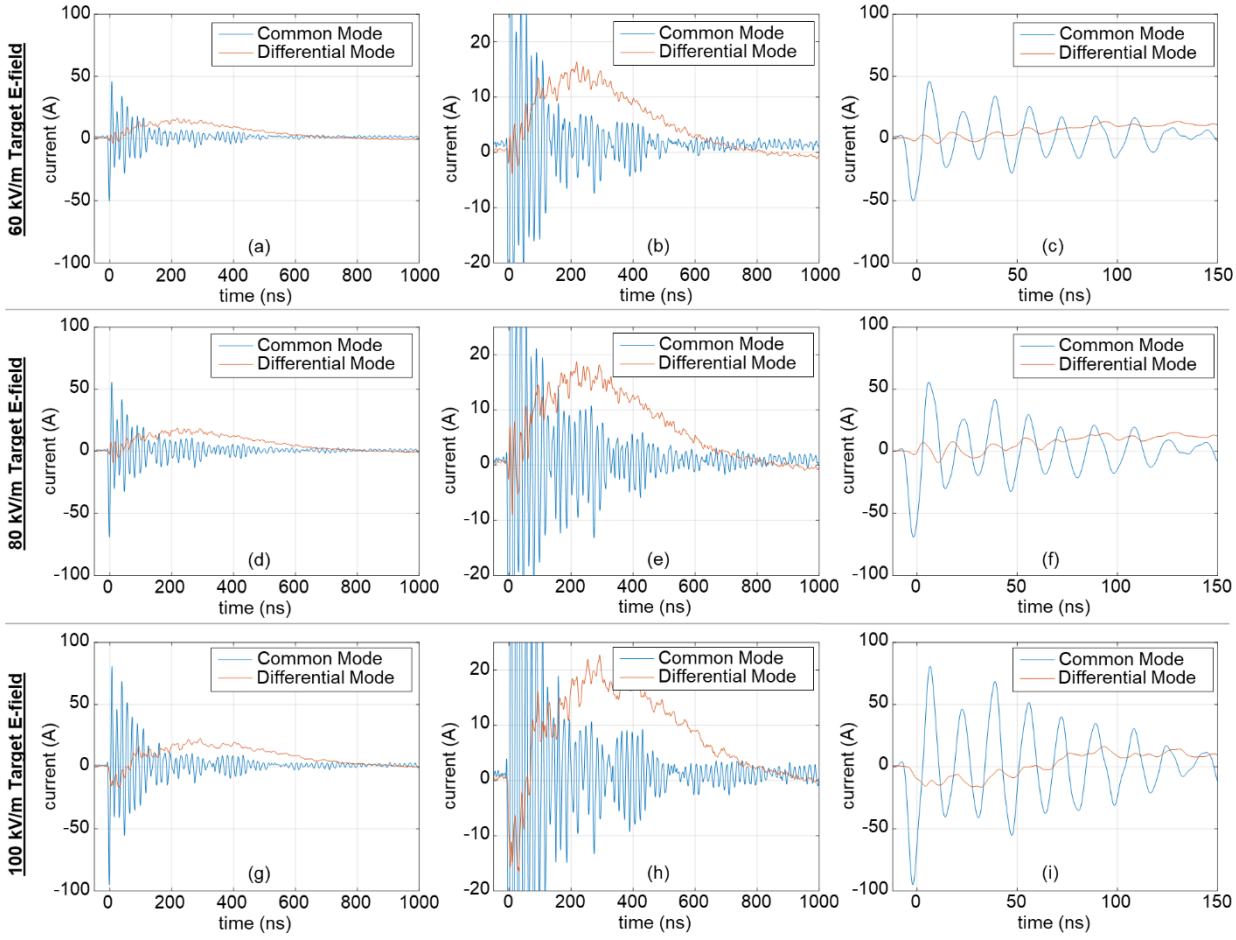

Figure 3-9. Module 8 coupled current measurements for (a) for 60 kV/m (b) with y-axis zoom on differential mode and (c) x-axis zoom on common mode, (d) for 80 kV/m (e) with y-axis zoom on differential mode and (f) x-axis zoom on common mode, and (g) for 100 kV/m (h) with y-axis zoom on differential mode and (i) x-axis zoom on common mode.

While the measured current values for every module in the horizontal orientation followed a similar trend, changing the module orientation had a significant effect on the strength of each coupled current. The currents measured for module 9 in vertical orientation are shown in Figure 3-10, organized in the same way as for module 8 in Figure 3-9.. The common mode current response is

seen to increase significantly with the module in the vertical orientation, exceeding -147.7–160.6 A (limited by scope settings) for the 100 kV/m response. Meanwhile the differential mode current is reduced, falling well under 15 A for the same pulse. This change in response is most likely due to the rotation of the module changing the orientation of the conductor path with respect to the incoming field. This difference is important for predicting the behavior of different PV module orientations and indicates that the manner in which the module is set up may be a factor when planning more resilient PV installations. Current measurements were also taken for the planar orientation of module 9 and showed lower currents in both common and differential mode than the other two orientations. The planar orientation results are not plotted here but are detailed in Table A-2.

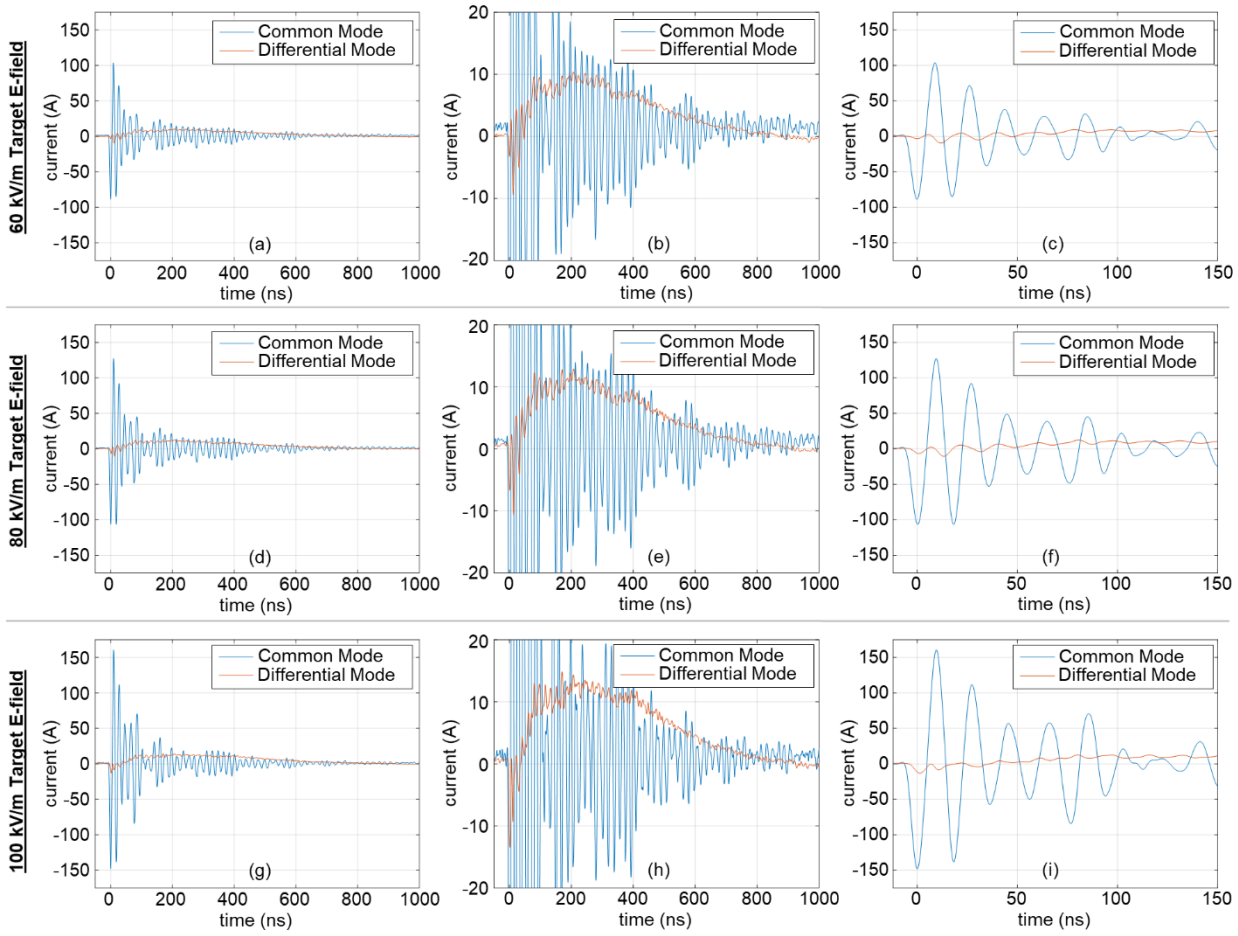

Figure 3-10. Module 9 coupled current measurements in vertical orientation (a) for 60 kV/m (b) with y-axis zoom on differential mode and (c) x-axis zoom on common mode, (d) for 80 kV/m (e) with y-axis zoom on differential mode and (f) x-axis zoom on common mode, and (g) for 100 kV/m (h) with y-axis zoom on differential mode and (i) x-axis zoom on common mode.

In addition to the current peak values, changing the orientation of the modules also gradually shifted the resonance frequency and the rise time of the common mode current. This may be due to a difference in module capacitance to the EMES ground plane for the different orientations, but the overall reason is not clear. Summary details of the common mode response are provided in Table 3-3. It should be noted that the filter used for the current calculation smoothed the rising edge of the common mode such that the filtered signal had consistent rise times across all three orientations. This was not the case for the original measurements, though the difference in rise time was small.

Table 3-3. Common mode response differences with module orientation

Module Orientation	Rise Time (before filter)	Rise Time (after filter)	Resonant Frequency	Peak Current ($\|I_{CM}\|_{max}$)[1]		
				60 kV/m	80 kV/m	100 kV/m
Horizontal	2.0-2.4 ns	2.8-3.0 ns	58.6 MHz	53.5 A	67.4 A	88.7 A
Vertical	3.2-3.4 ns		53.4 MHz	103.6 A	127.2 A	160.6 A
Planar	3.0-3.4 ns		61.8 MHz	29.2 A	29.6 A	42.3 A

[1] This is the approximate amplitude of the damped sine signal. For Horizontal orientation this was taken as the average peak of Modules 2 and 4-8. For Vertical and Planar orientation this was calculated for Module 9 alone.

The coupled current data in Table 3-3 and in Appendix A can be seen to scale with rough linearity with respect to the target field value from EMES, with the differential mode current behaving as an approximate double exponential signal while the common mode appears closer to a damped sine. These results can serve as an approximation of the coupled insults through the PV modules in future susceptibility testing or simulation of components in the PV module circuit.

4. CONCLUSIONS

Exposure of multicrystalline silicon photovoltaic modules to E1-like electromagnetic pulses of up to 100 kV/m (with a maximum measured pulse of 125 kV/m) indicated very minor observable module degradation or loss of function when compared against reference module data. This survivability was observed across 8 modules and 3 orientations with respect to the field polarization. The results suggest that multicrystalline silicon PV modules would be relatively unaffected by a HEMP event. Statistical fitting of the fill factors calculated from the module I-V curve traces suggested possible degradation with higher insult peaks, but this provides only a minor effect, if any, on the multicrystalline silicon module behavior and no indication of significant failure or changes. Other considerations of fill factor or peak power for the modules under test compared to a reference module showed little evidence of degradation. Following the initial testing and state of health measurements, a more thorough investigation of state of health was performed using flash I-V curve tracing and electroluminescence imaging, which is detailed in Appendix C. These follow-on measurements corroborated that there was little indication of electrical degradation or physical damage from the EMES electric field insults. A few small points of damage were observed and are most likely due to sample handling.

Coupled current measurements during testing showed peak differential mode currents up to approximately 20 A for a resistive load representative of a DC to AC inverter connected to the module. This differential mode current showed a slower response than the field impulse in all cases, with a duration of 500-1000 ns. Meanwhile the measured common mode current showed high frequency peaks exceeding 100 A for shots of 100 kV/m, though this was seen to decrease somewhat linearly with the peak field value. The common mode current was shown to be even higher for a more vertically-aligned PV cell. While these currents were not sufficient to damage the module or load, the conducted pulse will have to be considered for additional testing of inverters connected to PV modules to fully assess the resilience of a solar power generation station. Additional effects from multiple modules in series or different materials will also require future investigation.

REFERENCES

[1] Electromagnetic compatibility (EMC) – Part 2: Environment – Section 9: Description of HEMP environment – Radiated disturbance, IEC 61000-2-9:1996. International Electrotechnical Commission, Geneva, 1996.

[2] H.J. Hovel, Semiconductors and Semimetals, Volume II: Solar Cells, pub. Academic Press 1975, ISBN 0127521119

[3] Sandia National Laboratories, "Fast Rise-Time EMP Pulser," Sandia Technical Work Document, Department 1353 FREMP_TWD_Rev E.

APPENDIX A. DATA TABLES

A.1. Full EMES Shot Data

Table A-1 gives the full range of shots taken at EMES (organized by date) over the test period. This includes shots used for field mapping and characterization, designated as 'Field' in the Module # column. State of health measurements taken prior to any EMES pulse exposure are indicated by 'SOH' for the Shot #. Information is included for which module was tested, module orientation, measured peak power from the I-V curve trace when applicable, and measured module 3 reference peak power when applicable. Some reference measurements were compared against multiple sample measurements due to the small time between them and are indicated by a greyed-out cell. Irradiance data was collected starting with Shot #6 on 10/15 once a consistent setup for the I-V curve trace measurement was established. Prior state of health checks had the sample and control angled toward the sun directly and can only be compared to each other.

Table A-1. Full EMES Shot Data and State of Health Measurements

Date	Shot #[1]	Module #	Orientation	Illumination[2]	EMES Target Field[3] (kV/m)	EMES Actual Field (kV/m)	Sample Peak Power (W)	Module 3[4] Peak Power (W)	Sample Irradiance (W/m^2)	Module 3[4] Irradiance (W/m^2)
10/10	1	Field	-	-	50	39.9	-	-	-	-
10/10	2	Field	-	-	50	46.5	-	-	-	-
10/10	3	Field	-	-	50	55.8	-	-	-	-
10/10	4	Field	-	-	50	50.5	-	-	-	-
10/10	5	Field	-	-	50	50.7	-	-	-	-
10/10	6	Field	-	-	50	46.4	-	-	-	-
10/10	7	1	Horizontal	Dark	25	22.9	LEDs used. Invalid for I-V curve trace.			
10/10	8	1	Horizontal	Dark	25	22.9	LEDs used. Invalid for I-V curve trace.			
10/10	9	1	Horizontal	Dark	25	25.0	LEDs used. Invalid for I-V curve trace.			
10/14	SOH	1	-	-	-	-	179.0	194.4	-	-
10/14	1	1	Horizontal	Dark	25	27.8	214.5	-	-	-
10/14	2	1	Horizontal	Illuminated	25	27.5	154.0	-	-	-
10/14	3	1	Horizontal	Dark	25	27.5	-	-	-	-
10/14	4	1	Horizontal	Dark	25	28.3	231.9	228.1	-	-
10/14	5	1	Horizontal	Dark	35	37.5	228.8	-	-	-
10/14	6	1	Horizontal	Dark	35	35.6	236.5	-	-	-
10/14	7	1	Horizontal	Dark	50	45.7	236.5	225.3	-	-
10/14	8	1	Horizontal	Illuminated	50	44.8	253.1	250.7	-	-
10/15	SOH	1	-	-	-	-	167.3	178.8	-	-
10/15	1	Field	-	-	50	62.0	-	-	-	-
10/15	2	Field	-	-	50	62.7	-	-	-	-
10/15	3	Field	-	-	50	51.3	-	-	-	-
10/15	4	Field	-	-	50	51.3	-	-	-	-
10/15	5	Field	-	-	50	50.6	-	-	-	-
10/15	6	1	Horizontal	Dark	50	45.9	166.9	194.9	765.40	784.79

Date	Shot #[1]	Module #	Orientation	Illumination[2]	EMES Target Field[3] (kV/m)	EMES Actual Field (kV/m)	Sample Peak Power (W)	Module 3[4] Peak Power (W)	Sample Irradiance (W/m^2)	Module 3[4] Irradiance (W/m^2)
10/15	7	1	Horizontal	Dark	65	61.4	222.9	-	904.36	-
10/15	8	1	Horizontal	Dark	65	56.4	-	-	-	-
10/15	9	1	Horizontal	Dark	65	58.2	209.0	-	-	-
10/15	10	1	Horizontal	Dark	65	67.2	237.7	215.2	884.05	875.85
10/15	11	1	Horizontal	Dark	80	81.6	250.3	252.6	594.93	596.24
10/15	12	1	Horizontal	Dark	100	117.8	208.0	199.6	598.65	599.43
10/15	13	1	Horizontal	Illuminated	100	125.0	167.8	161.5	604.47	604.50
10/16	1	Field	-	-	60	71.7	-	-	-	-
10/16	2	Field	-	-	60	68.5	-	-	-	-
10/16	3	Field	-	-	80	85.8	-	-	-	-
10/16	4	Field	-	-	80	93.5	-	-	-	-
10/16	5	Field	-	-	80	81.4	-	-	-	-
10/16	6	Field	-	-	80	86.1	-	-	-	-
10/16	7	Field	-	-	100	118.0	-	-	-	-
10/16	8	Field	-	-	100	114.6	-	-	-	-
10/16	9	Field	-	-	100	110.0	-	-	-	-
10/16	SOH	2	-	-	-	-	96.8	86.1	325.24	336.35
10/16	10	2	Horizontal	Dark	60	64.8	225.0	221.8	934.67	934.98
10/16	11	2	Horizontal	Dark	80	77.4	233.0	200.8	937.43	937.16
10/16	12	2	Horizontal	Dark	100	106.3	254.0	209.9	925.30	920.62
10/16	SOH	4	-	-	-	-	234.4	209.9	913.97	920.62
10/16	SOH	5	-	-	-	-	261.4	209.9	897.50	920.62
10/16	13	4	Horizontal	Dark	60	65.3	259.2	220.2	554.03	542.22
10/16	14	5	Horizontal	Dark	60	59.7	256.8	210.6	530.35	516.99
10/16	15	4	Horizontal	Dark	80	79.6	246.9	226.4	501.24	477.68
10/16	16	5	Horizontal	Dark	80	75.9	247.6	226.4	478.32	477.68
10/16	17	4	Horizontal	Dark	100	104	229.0	227.1	458.75	449.99
10/16	18	5	Horizontal	Dark	100	97.2	236.3	227.1	430.92	449.99
10/16	SOH	6	-	-	-	-	236.9	227.1	429.42	449.99
10/16	19	6	Horizontal	Dark	60	63.4	245.5	220.1	402.75	398.88
10/16	20	6	Horizontal	Dark	80	82.2	223.8	217.5	365.26	357.33
10/16	21	6	Horizontal	Dark	100	105.1	210.1	200.8	324.91	320.67
10/17	SOH	7	-	-	-	-	56.7	54.2	177.47	212.85
10/17	1	7	Horizontal	Dark	60	61.7	94.3	95.8	291.20	296.27
10/17	2	7	Horizontal	Dark	80	82.7	35.8	34.2	344.52	322.24
10/17	3	7	Horizontal	Dark	100	108.5	34.8	26.7	386.14	390.78
10/17	SOH	8	-	-	-	-	282.1	260.7	498.30	573.38
10/17	SOH	9	-	-	-	-	267.0	260.7	626.64	573.38

Date	Shot #[1]	Module #	Orientation	Illumination[2]	EMES Target Field[3] (kV/m)	EMES Actual Field (kV/m)	Sample Peak Power (W)	Module 3[4] Peak Power (W)	Sample Irradiance (W/m^2)	Module 3[4] Irradiance (W/m^2)
10/17	4	8	Horizontal	Dark	60	62.2	124.1	110	493.58	238.53
10/17	5	9	Vertical	Dark	60	65.3	290.1	271.6	493.65	569.67
10/17	6	9	Planar	Dark	60	71.3	260.3	272.0	504.51	500.21
10/17	7	8	Horizontal	Dark	80	85.2	151.8	185.9	468.34	478.07
10/17	8	9	Vertical	Dark	80	83.8	83.4	162.5	430.88	412.10
10/17	9	9	Planar	Dark	80	76.7	78.9	126.8	413.55	415.81
10/17	10	8	Horizontal	Illuminated	100	108.0	206.5	195.3	370.39	364.15
10/17	11	9	Vertical	Illuminated	100	110.5	224.9	191.1	296.08	224.70
10/17	12	9	Planar	Illuminated	100	112.9	218.7	171.4	294.12	272.99
10/17	13	9	Horizontal	Dark	100	102.5	-	-	-	-

[1] Shot # refers to the sequential number of shots for a given date. Shots designated as 'Field' shots were taken of the empty test chamber to characterize the peak field and define the pulser settings for the subsequent tests.
[2] Illumination refers to whether the LED arrays directed at the module were illuminated or dark. Illumination was used for visualization only and had no observable effect on module response.
[3] The target field is the peak electric field value that was intended by the EMES pulser settings based on past electric field measurements. EMES allows a 10-15% variation between the target field and actual field peak.
[4] The reference I-V curves were taken from Module 3, which had no EMES exposure, for comparison against the sample.

A.2. Full Coupled Current Peak Data

The full coupled current in differential and common mode is given in Table A-2. Most module 1 shots were used to calibrate the CT attenuation and scope settings and therefore were not usable for comparison of current data. A noise shot at 100 kV/m (actual peak 102.5 kV/m) was taken with module 9 in the test chamber but not connected to the CTs (Shot #13 on 10/17). This produced the inherent coupling of the field to the CTs independent of PV module coupling, which was lower for both common and differential mode currents and likely had little impact on the measured responses for the connected modules. The noise shot was also used to define the noise floor when selecting appropriate filters for the CT data. For the current ranges, the calculated current using the frequency dependent impedance of the CTs and low-pass filters is given.

Table A-2. Full Coupled Current Peak Data

Date	Shot #	Module #	Orientation	Illumination	Target Field (kV/m)	Actual Field (kV/m)	I_{Range}, Differential Mode (A)	I_{Range}, Common Mode (A)
10/16	10	2	Horizontal	Dark	60	64.8	-8.68 – 16.0	-54.8 – 53.6
10/16	11	2	Horizontal	Dark	80	77.4	-12.9 – 18.2	-68.2 – 61.8
10/16	12	2	Horizontal	Dark	100	106.3	-11.3 – 20.6	-87.3 – 72.8
10/16	13	4	Horizontal	Dark	60	65.3	-11.4 – 16.3	-59.0 – 57.4
10/16	15	4	Horizontal	Dark	80	79.6	-3.30 – 17.3	-67.2 – 68.6
10/16	17	4	Horizontal	Dark	100	104	-11.9 – 20.8	-87.0 – 73.0
10/16	14	5	Horizontal	Dark	60	59.7	-3.02 – 15.2	-52.3 – 47.7
10/16	16	5	Horizontal	Dark	80	75.9	-6.71 – 17.7	-61.8 – 60.2

Date	Shot #	Module #	Orientation	Illumination	Target Field (kV/m)	Actual Field (kV/m)	I_{Range}, Differential Mode (A)	I_{Range}, Common Mode (A)
10/16	18	5	Horizontal	Dark	100	97.2	-6.74 – 18.7	-78.8 – 68.3
10/16	19	6	Horizontal	Dark	60	63.4	-7.32 – 16.1	-55.1 – 50.2
10/16	20	6	Horizontal	Dark	80	82.2	-8.55 – 19.1	-67.9 – 59.0
10/16	21	6	Horizontal	Dark	100	105.1	-14.3 – 20.6	-90.9 – 76.8
10/17	1	7	Horizontal	Dark	60	61.7	-5.73 – 15.9	-49.6 – 43.8
10/17	2	7	Horizontal	Dark	80	82.7	-4.61 – 18.6	-70.1 – 59.0
10/17	3	7	Horizontal	Dark	100	108.5	-7.70 – 20.9	-93.0 – 77.1
10/17	4	8	Horizontal	Dark	60	62.2	-3.89 – 16.4	-50.2 – 46.0
10/17	7	8	Horizontal	Dark	80	85.2	-9.04 – 18.8	-69.0 – 55.7
10/17	10	8	Horizontal	Illuminated	100	108.0	-16.4 – 22.7	-95.1 – 80.7
10/17	5	9	Vertical	Dark	60	65.3	-9.4 – 10.4	-88.6 – 103.6
10/17	8	9	Vertical	Dark	80	83.8	-10.6 – 12.9	-106.4 – 127.2
10/17	11	9	Vertical	Illuminated	100	110.5	-13.0 – 14.7	-147.7 – 160.6
10/17	6	9	Planar	Dark	60	71.3	-5.66 – 6.51	-27.1 – 29.2
10/17	9	9	Planar	Dark	80	76.7	-4.76 – 5.99	-29.0 – 29.6
10/17	12	9	Planar	Illuminated	100	112.9	-5.46 – 9.00	-42.1 – 42.3
10/17	13	Noise	Horizontal	Dark	100	102.5	-5.98 – 7.68*	-14.2 – 17.1*

*The current response from the observed noise shot showed ringing in both cases rather than the common damped sine wave or differential mode double exponential seen for all measurements with the load connected.

APPENDIX B. I-V CURVE TRACE MEASUREMENT ANALYSIS

This appendix presents all state of health I-V curves measured over the course of testing. The first three shots on module 1 were conducted at 25 kV/m with the LEDs used as illumination for the SOH check and prior to taking measurements from an experimental control. The I-V curves after each shot are shown in Figure B-1a compared to the curve taken prior to testing, designated as the state of health or SOH curve. For the second shot, the I-V curve showed no notable current at first but recovered to the plotted level after 15 minutes, while the I-V curve after the third shot showed no recovery even after 15 minutes. While these initial curves imply degradation of the PV module function with each shot, subsequent measurements of the module under external lighting showed no observable loss of function when compared to modules that had not yet been exposed to pulsed fields, as seen in Figure B-1b. It was determined that LED illumination was insufficient to excite module behavior and was therefore not used for additional state of health checks.

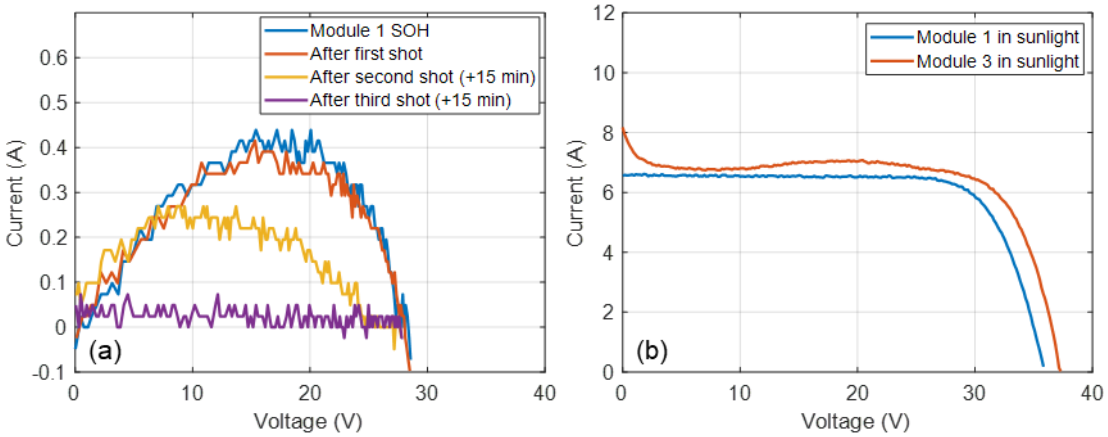

Figure B-1. Module 1 state of health measurements (a) under LED illumination between 25 kV/m shots and (b) under external illumination compared to module 3.

Subsequent measurements of module 1 and all other modules were performed under direct sunlight illumination. The I-V curves for module 1 compared to module 3 measurements taken in the same time frame are shown in Figure B-2. The shots for module 1 correspond to shots #6-13 on 10/15 in Table A-1. Not every I-V curve trace for module 1 was accompanied by a trace in module 3, and the measurements in Figure B-2b correspond to reference measurements taken after shots #6 and #10-13. Here it's observed that the overall current levels of module 1 have an upward trend as the peak field increases from 50 kV/m to 80 kV/m, then decreases for the 100 kV/m shots. The same trend is shown for module 3 measured at the same time as the indicated shots, which indicates that these trends are likely from ambient conditions for the I-V curve measurements and not a sign of change in module behavior.

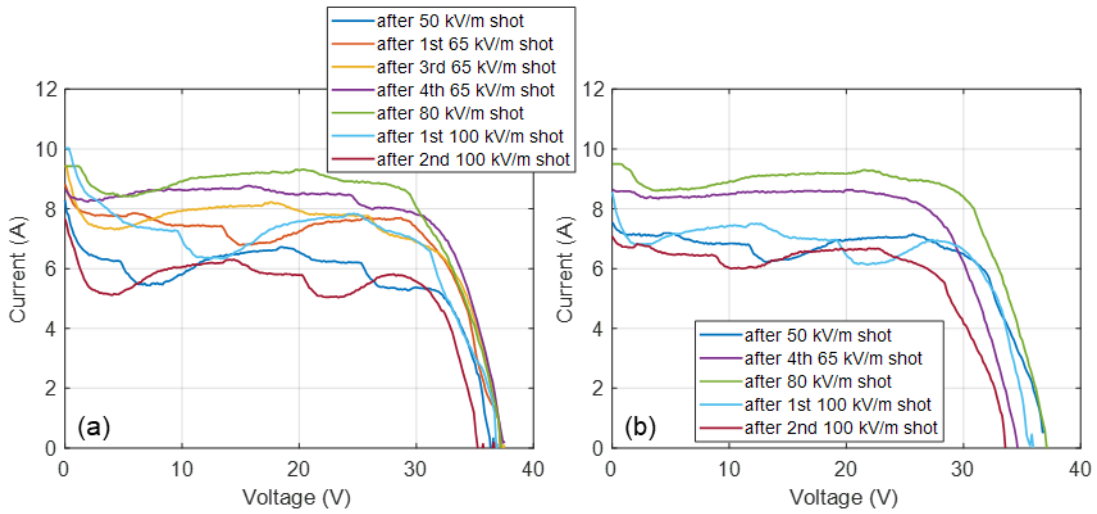

Figure B-2. State of health measurements (a) for module 1 over the course of testing (shots #6-13 on 10/15) and (b) module 3 during the same time.

The I-V curves for module 2 and associated module 3 measurements are shown in Figure B-3. These measurements correspond to shots #10-12 on 10/16 in Table A-1. For both module 1 and module 3, the measurement taken prior to testing shows a low overall current and oscillating behavior. This is most likely partial shading of the modules due to cloud cover and early morning conditions. Overall the two modules show the same trend with no clear indication of performance degradation.

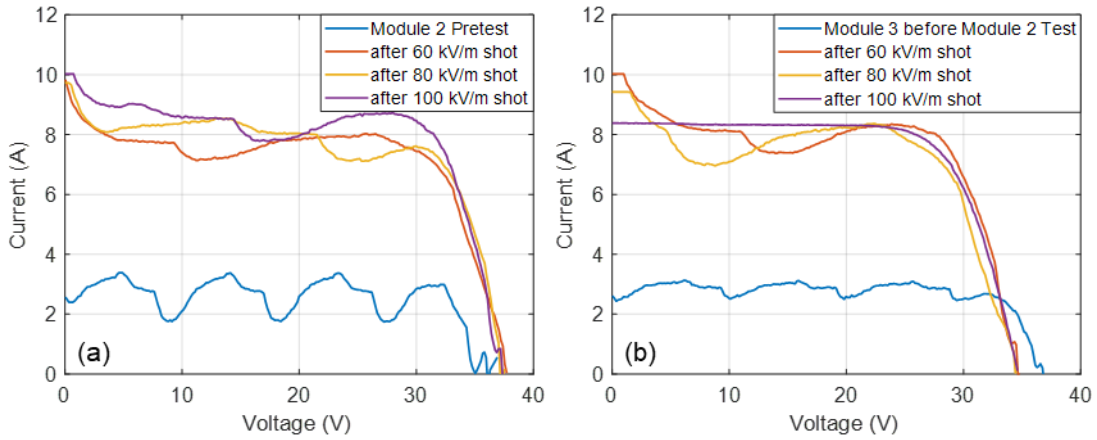

Figure B-3. State of health measurements (a) for module 2 over the course of testing (shots #10-12 on 10/16) and (b) module 3 during the same time.

The I-V curves for module 4 and associated module 3 measurements are shown in Figure B-4. These tests were performed in sequence with the tests on module 5, which are plotted in Figure B-5. The shots on module 4 correspond to shots #13, 15, and 17 on 10/16 in Table A-1, and the shots on module 5 correspond to shots #14, 16, and 18. Due to the sequential nature of these sweeps, some of the module 3 measurements are correlated to both module 4 and module 5 I-V curves. In both cases there is no observable degradation of the behavior of the module being tested, and the overall trends of both sets of measurements follow the same trend as the module 3 measurements taken during the same time.

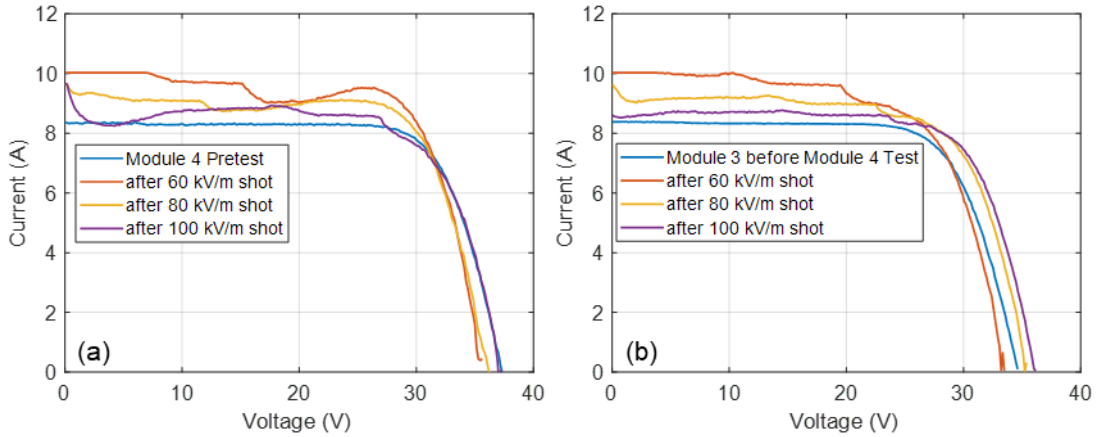

Figure B-4. State of health measurements (a) for module 4 over the course of testing (shots #13, 15, and 17 on 10/16) and (b) module 3 during the same time.

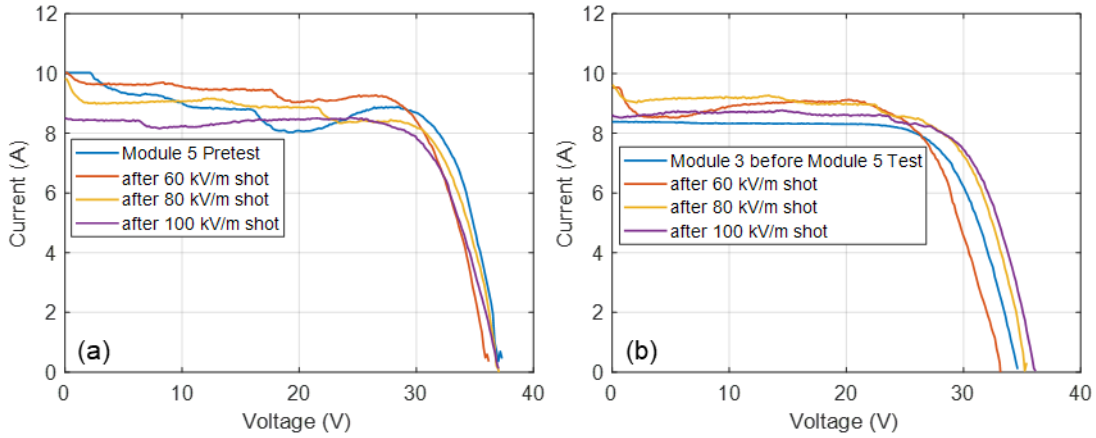

Figure B-5. State of health measurements (a) for module 5 over the course of testing (shots #14, 16, and 18 on 10/16) and (b) module 3 during the same time.

The I-V curves for module 6 and associated module 3 measurements are shown in Figure B-6 and correspond to shots #19-21 on 10/16 in Table A-1. While the state of health measurements show a negative trend in the I-V curve current with shot progression, the same trend is seen for the module 3 measurements and is most likely due to ambient conditions and not indicative of performance degradation.

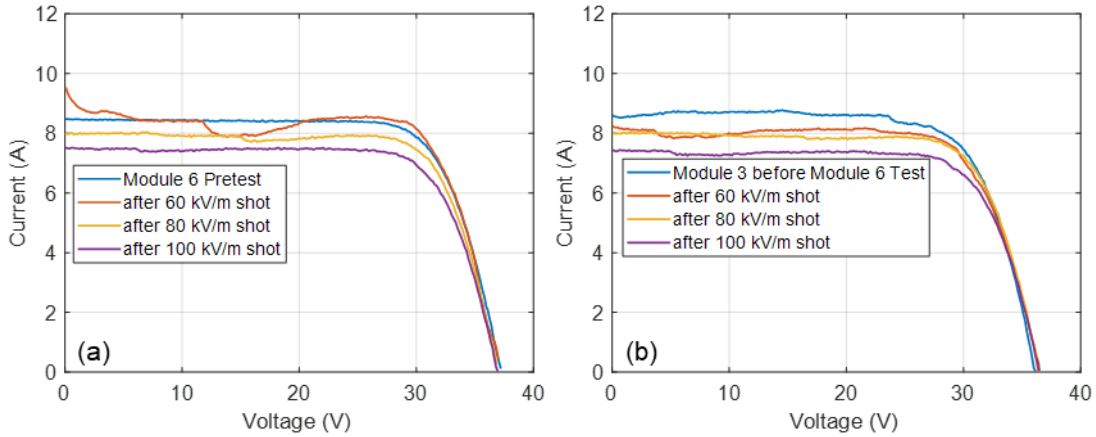

Figure B-6. State of health measurements (a) for module 6 over the course of testing (shots #19-21 on 10/16) and (b) module 3 during the same time.

The I-V curves for module 7 and associated measurements of module 3 are shown in Figure B-7 and correspond to shots #1-3 on 10/17 in Table A-1. All measurements on 10/17 were subject to varying lighting conditions due to cloud cover. Additionally, the I-V curves for module 7 were taken in early morning lighting conditions, resulting in much lower overall current and power values than for other modules. However, comparison against module 3 measurements shows consistent trends and levels with the untested module and no signs of performance degradation.

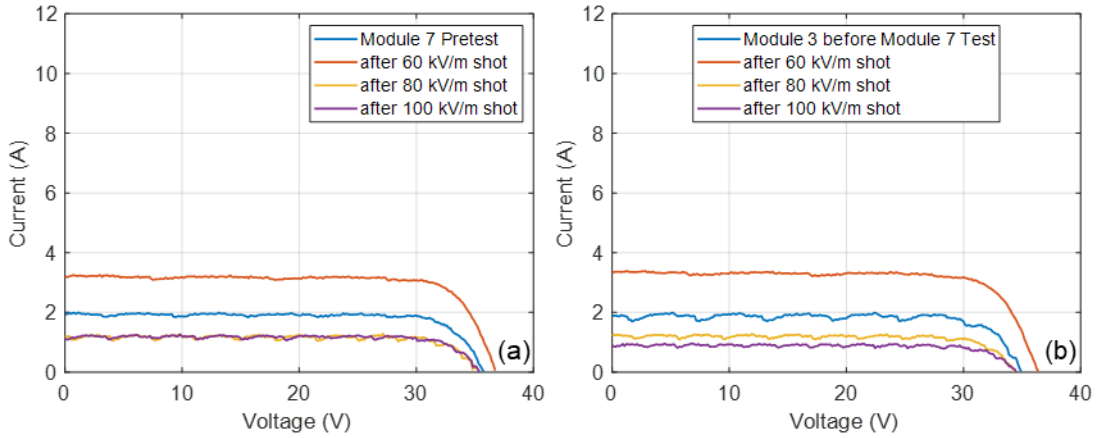

Figure B-7. State of health measurements (a) for module 7 over the course of testing (shots #1-3 on 10/17) and (b) module 3 during the same time.

The I-V curves for module 8 and associated measurements of module 3 are shown in Figure B- and correspond to shots #4, 7, and 10 on 10/17 in Table A-1. There is a wide variation in the current levels of the I-V curves between the different shots without a clear trend based on shot progression due to the variation in lighting condition. Similar curves are seen between module 8 and module 3 across the series of shots. The one exception is the 80 kV/m measurements, which are likely due to an unexpected shift in lighting conditions. The I-V curves taken after the 100 kV/m shot are once again aligned, indicating general agreement.

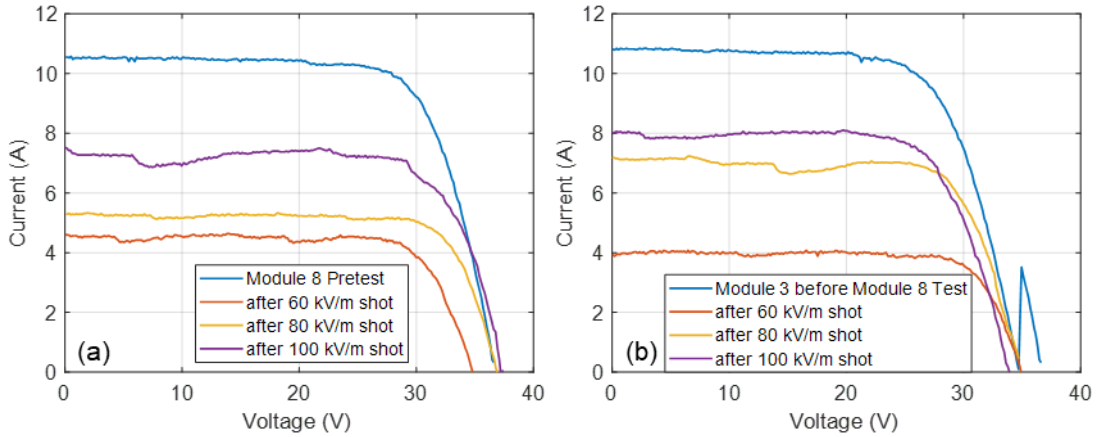

Figure B-8. State of health measurements (a) for module 8 over the course of testing (shots #4, 7, and 10 on 10/17) and (b) module 3 during the same time.

The I-V curves for module 9 and associated measurements of module 3 are shown in Figure B- and correspond to shots #5, 6, 8, 9, 11, and 12 on 10/17 in Table A-1. These measurements were performed in sequence with the measurements on module 8, and the orientation was alternated between vertical and planar orientations of the module at each field level. Like the module 8 measurements, a discrepancy is seen between the 80 kV/m shot measurements between module 9 and module 3, while the two modules are relatively close after the 100 kV/m shot. This implies inconsistent lighting levels at the time that the 80 kV/m shots were performed on modules 8 and 9, whereas the state of health taken after the 100 kV/m shots is consistent between the two modules and module 3.

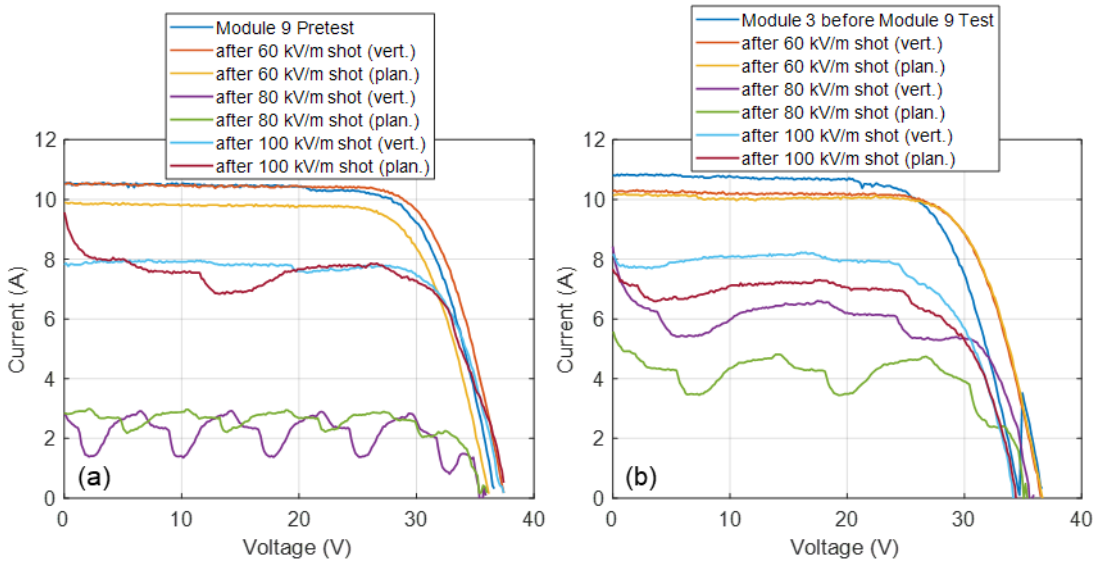

Figure B-9. State of health measurements (a) for module 9 over the course of testing (shots #5, 6, 8, 9, 11, and 12 on 10/17) and (b) module 3 during the same time.

In general, all I-V curves followed the same trends as the module 3 measurements with a few exceptions. No clear signs of performance degradation or other altered state of the PV modules were observed.

APPENDIX C. FLASH I-V CURVE AND ELECTROLUMINESCENCE TESTS

C.1. Introduction

Following the TEM wave insult testing at EMES, all PV modules were subsequently tested in Sandia's Photovoltaic Systems Evaluation Laboratory (PSEL) using two methods: flash I-V curve measurements and electroluminescence (EL) imaging. This appendix presents the results of these tests and discusses what the test results might indicate regarding the effects on the PV modules of HEMP exposure.

During the outdoor I-V curve measurements of these PV modules, temperature control of the modules was not possible, which presented some difficulty due to fill factor dependence on module temperature. In the PSEL testing, the modules were not directly temperature-controlled but were allowed to thermally equilibrate in a temperature-controlled laboratory. The flashed nature of the light exposure did not lead to a significant change in temperature. In this way, the temperatures of the modules were constrained to a narrow range to mostly eliminate their impact on module fill factor.

Outdoor I-V curve measurements were taken before and after the EMES TEM insult, but the indoor tests were taken only after eight of the nine test modules were exposed to the TEM insult. Thus, for the indoor tests, comparisons must be made between TEM-exposed modules and the reference module that was not exposed to TEM. PV modules contain natural manufacturing variances from module to module, and in the indoor tests those variances may mask any effects from the TEM insult.

The only solar exposure these modules received prior to the testing in the PSEL was that which they received during the outdoor I-V curve measurements taken before and after the EMP exposure.

C.2. Flash I-V curve tests

The eight test modules and one reference module were thermally equilibrated in the PSEL for 24 hours prior to the flash testing. Then, each module was flash tested on the PSEL's Class AAA Spire 4600 SLP Solar Simulator. The duration of each flash was 97 ms. The number of data points in each collected I-V curve ranged from 4032 to 4080, with an average of 4068.

The modules were flash-tested using Standard Test Conditions (1 kW/m^2 irradiance with an AM 1.5 global spectrum). Spectral corrections were not applied in this case. During the testing, the backsheet temperature of each module was monitored using a four-wire RTD probe. The module temperatures varied from 24.6 °C to 25.4 °C. The measured I-V curve results were corrected to the Standard Test Conditions temperature of 25 °C using the modules' thermal coefficients.

The results of the flash I-V curve testing are given numerically in Table C-1, and a plot of the measured I-V curves is given in Figure C-1. The reference module that was not exposed to any EMP is Module ID #3. The parameter variations between modules are well within the expected range of normal PV module variability based on manufacturing and other module-module differences. There is no discernable decrease in fill factor—in fact, all eight EMP-exposed modules have a higher fill factor than the reference module[1]. The distribution of fill factors among this sample set is rather tight; the average fill factor is 76.73 and the standard deviation is 0.24.

[1] This is probably due to a higher number of cracks in the reference module than in any of the EMP-exposed modules—see the EL results in the next section.

Table C-1. Module parameters measured during the flash I-V testing. The manufacturer-provided datasheet values are also listed for comparison.

Module ID	I_{sc} (A)	V_{oc} (V)	I_{mp} (A)	V_{mp} (V)	P_{mp} (W)	FF (%)	Eff. (%)	Ω @ V_{oc}	Ω @ I_{sc}	Temp (°C)
1	9.059	37.86	8.605	30.58	263.18	76.7	16.20	0.462	363	25.2
2	9.086	37.85	8.640	30.47	263.20	76.5	16.20	0.471	444	24.9
3	9.109	37.88	8.612	30.55	263.03	76.2	16.20	0.465	255	24.9
4	9.102	37.96	8.652	30.69	265.47	76.9	16.30	0.461	387	24.9
5	9.083	37.90	8.642	30.64	264.77	76.9	16.30	0.463	288	24.9
6	9.109	37.95	8.663	30.68	265.75	76.9	16.40	0.464	287	24.9
7	9.110	37.93	8.660	30.70	265.79	76.9	16.40	0.457	182	24.9
8	9.087	37.94	8.639	30.70	265.14	76.9	16.30	0.459	141	24.9
9	9.102	37.92	8.638	30.66	264.93	76.7	16.30	0.465	237	25.3
Datasheet	**9.07**	**38.16**	**8.5**	**30.59**	**260**	**75.1**	**15.98**	**-**	**-**	**-**

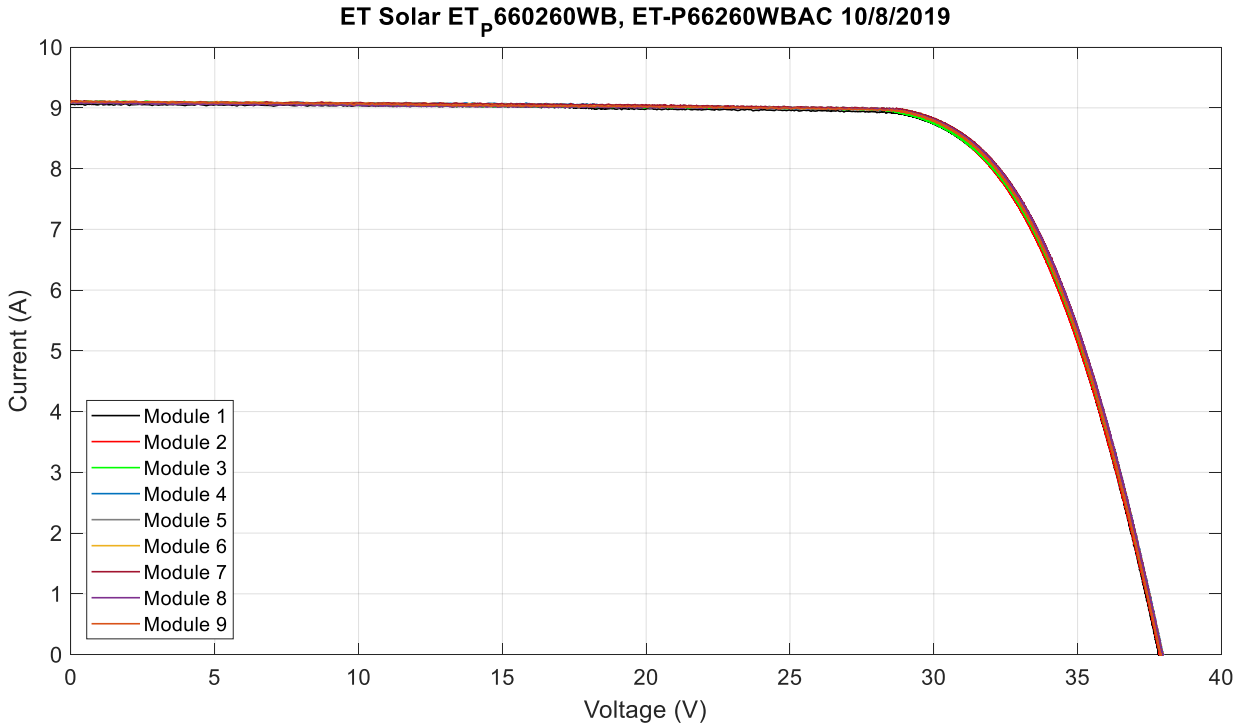

Figure C-1. Plots of the I-V curves of all nine tested modules (eight EMP-exposed modules plus one reference) from the flash I-V curve testing

Within the limits of this experiment, these results support the conclusion that the simulated EMP did not cause any immediate damage or have any near-term negative impacts on PV module performance.

C.3. Electroluminescence imaging

EL imaging works on the principle that solar cells can be operated as LEDs—albeit with low efficiency due to being a separate function from their intended design. If a voltage and current are applied to the cells, they will produce light with photon energies in a range just above the band gap of silicon. That light can be detected and used to produce a map of the electrical activity of the cells within a module. This is a powerful diagnostic technique that allows one to readily see various forms of damage or changes and where they occurred in the module.

The EL images are made in a light-tight dark room. The images are recorded with a Finger Lakes astronomical 16 megapixel camera with a 35 mm lens. All EL images were recorded with a long-pass filter (88% at 900 nm). The modules were biased with a Sorenson ELM150-20E DC power supply. For each module, two images were acquired: one at 80% of rated I_{SC} and the other at 20% of rated I_{SC}. These images highlight the series and shunt resistance effects respectively. Each of the images is an average of two captured frames. Exposure periods were not optimized to obtain balanced histograms or to avoid under- or over-saturation, but the same exposure periods were used for all modules to yield relative differences in luminescence (51.2 seconds and 3.41 minutes).

The captured EL images are shown in Figure C-2 through Figure C-10. In each figure, the low-current image is shown on the left and the high-current image on the right. The EL images for the reference module (#3) are shown in Figure C-4.

The PSEL investigators identified a number of cracks in the cells in these modules. In particular, the reference module showed several cracked cells. Modules #7 and #8 also showed some cracked cells. As noted earlier, the reference module had the lowest fill factor of the group, but modules #7 and #8 had two of the highest fill factors out of the group. It is possible that the cracks in the reference module could have an impact on module electrical performance that is larger than the impacts caused by EMP exposure, and thus the effects of the cracks could potentially mask any impacts of the EMP exposure. However, any impact on the modules exposed to EMP in this work would still fall within normal deviations of the module performance.

The EL images have a generally "speckled" appearance, which is due to the fact that these are multicrystalline Si modules with typical grain-to-grain differences in electrical activity. The "speckled" appearance is thus normal for this module type.

It was believed that if there were a negative impact on the modules' electrical performance caused by the EMP exposure, perhaps due to a photon-activated defect or similar effects, then one might see such defects as darker regions in the EL images. In this experiment, the comparison between the EMP-exposed modules and the reference module does not show any obvious impacts on electrical activity from the EMP exposure. The images do not show any readily-apparent darkening or expansion of any of the defect patterns, deviations from the typical patterns in this type of module, or overall dimming of the images that might occur if there were widespread EMP-induced damage[2]. The cracks seen in some of the TEM-exposed modules almost certainly occurred during handling and were not caused by the TEM exposure.

[2] These would also have shown up in the module fill factors.

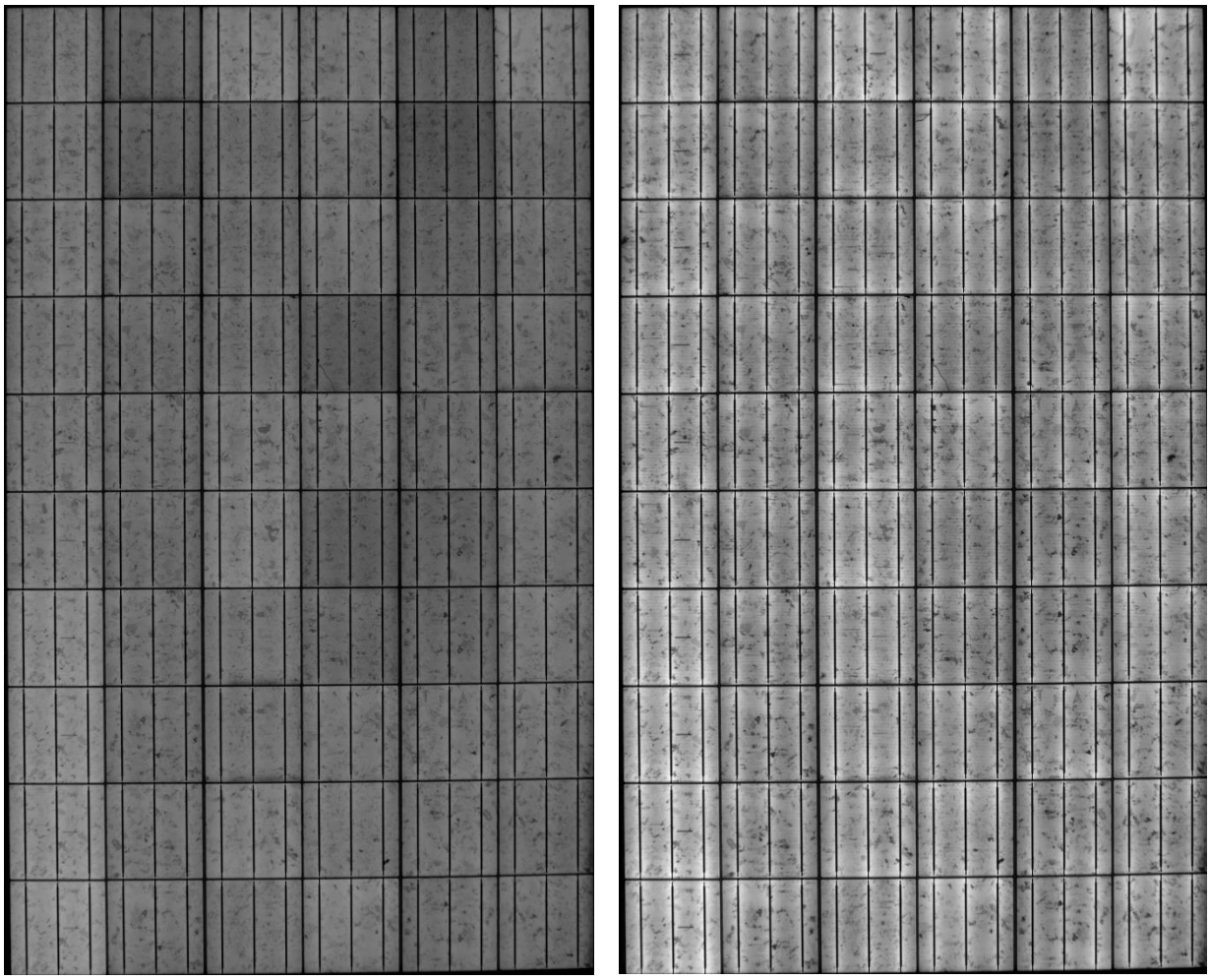

Figure C-2. EL images of Module #1. Left = low current, right = high current.

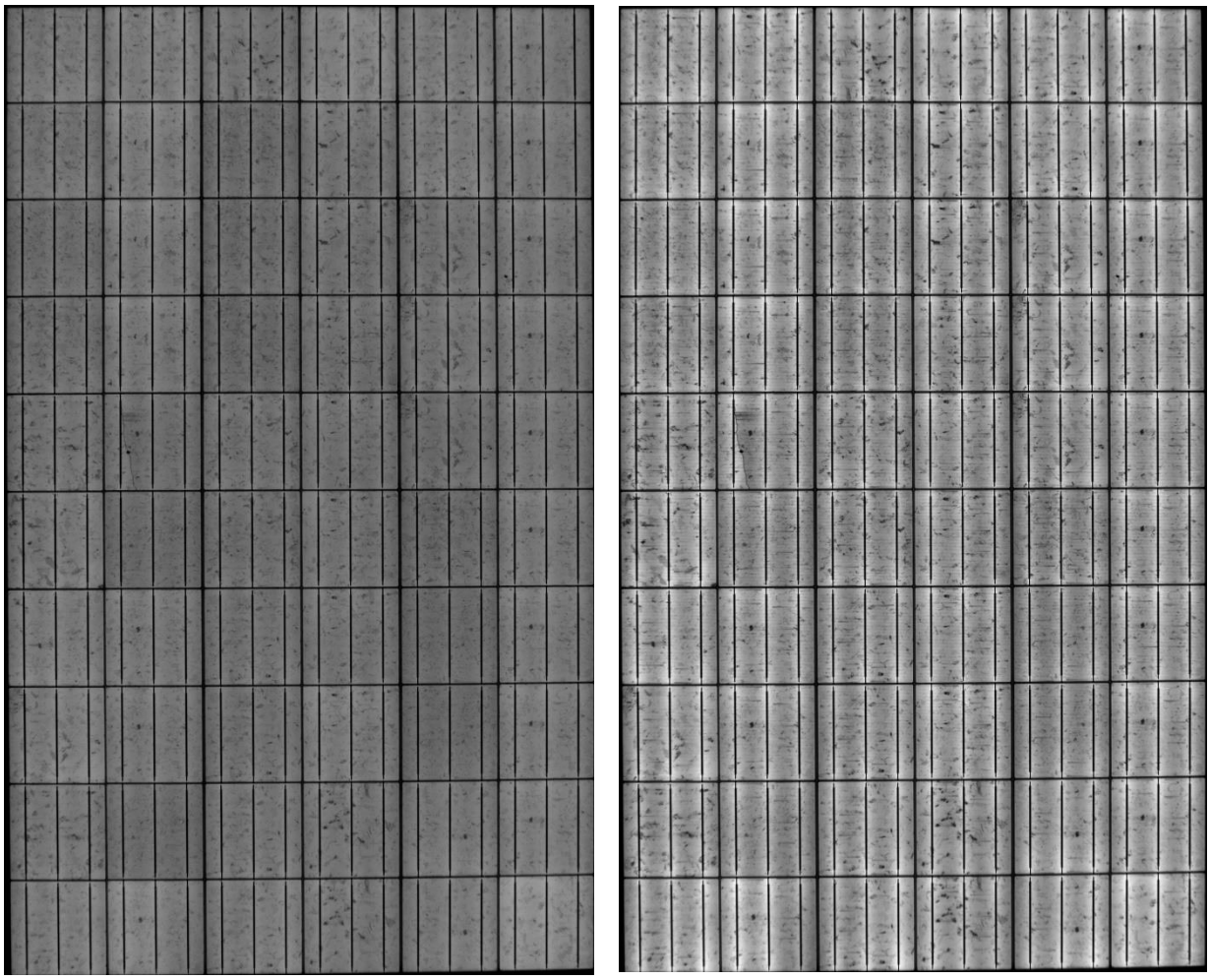

Figure C-3. EL images of Module #2. Left = low current, right = high current.

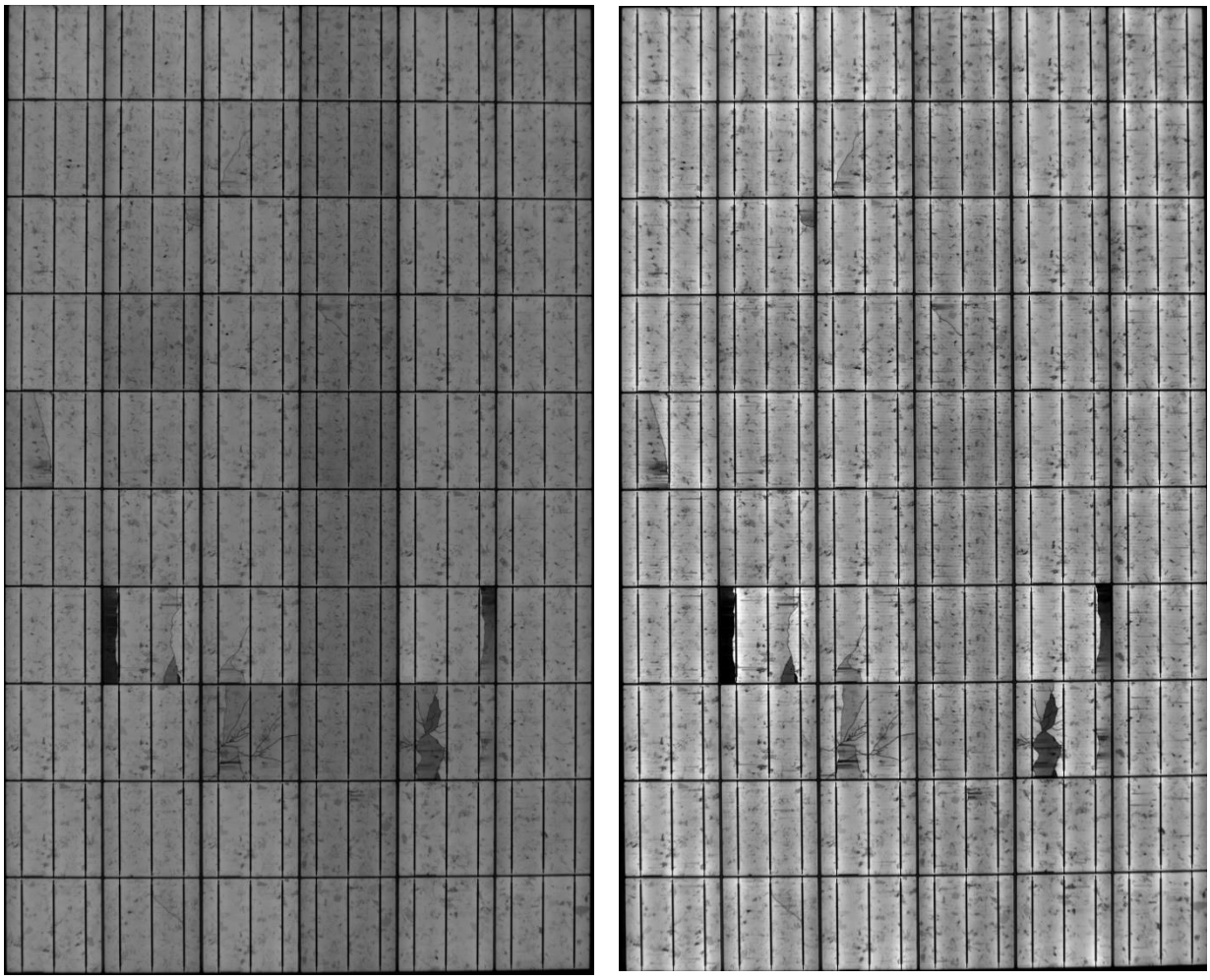

Figure C-4. EL images of Module #3 (the reference module that did not receive EMP exposure). Left = low current, right = high current.

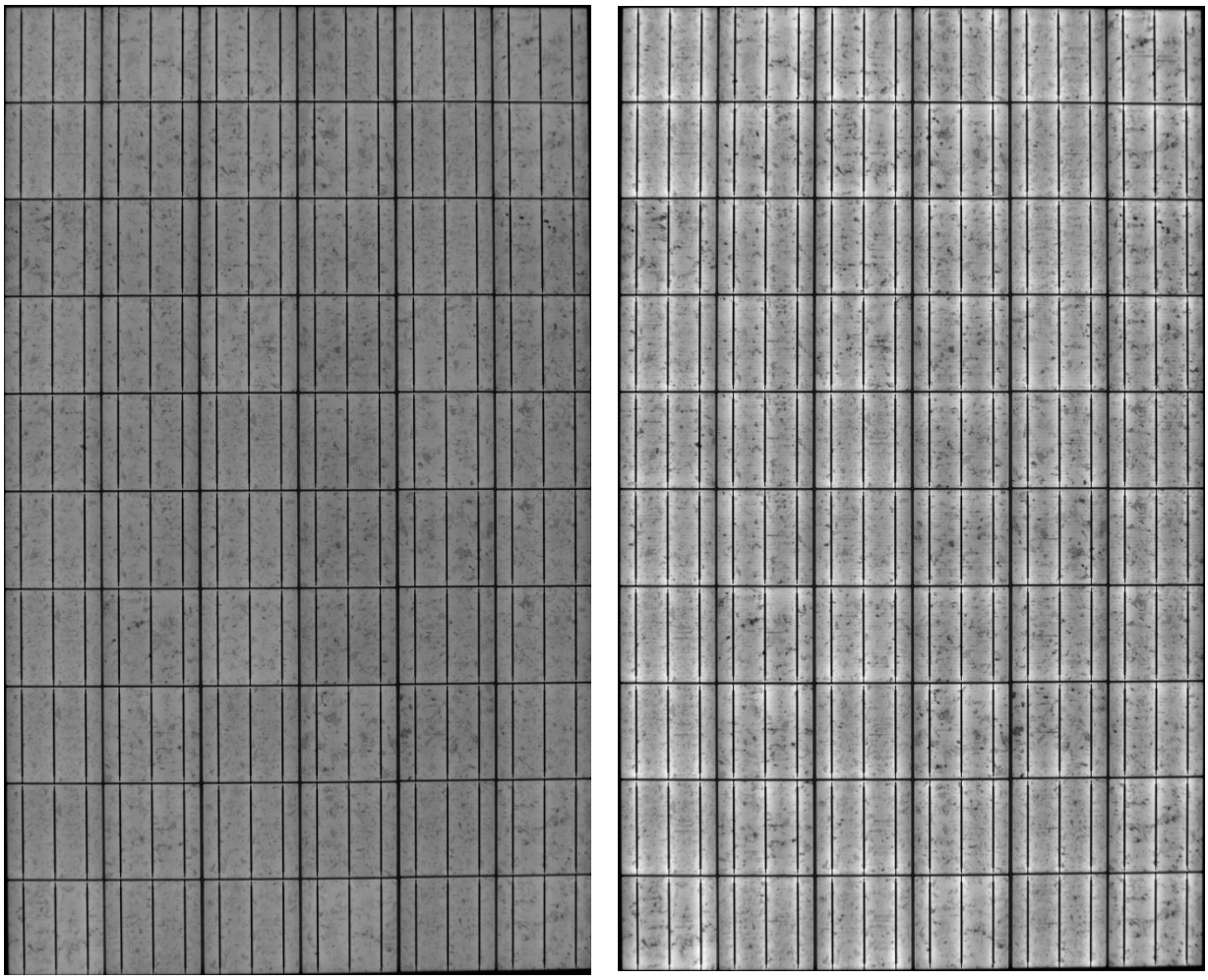

Figure C-5. EL images of Module #4. Left = low current, right = high current.

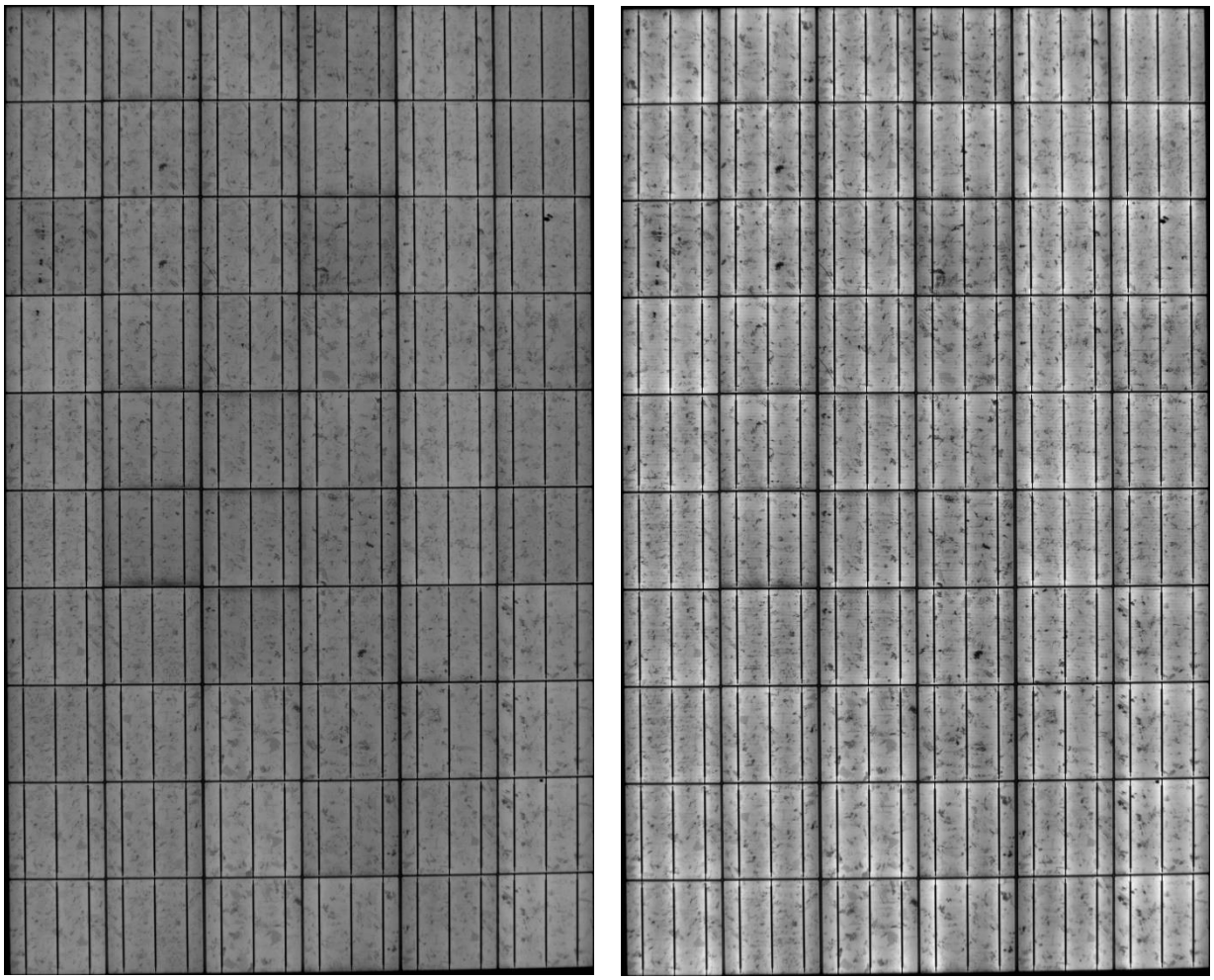

Figure C-6. EL images of Module #5. Left = low current, right = high current.

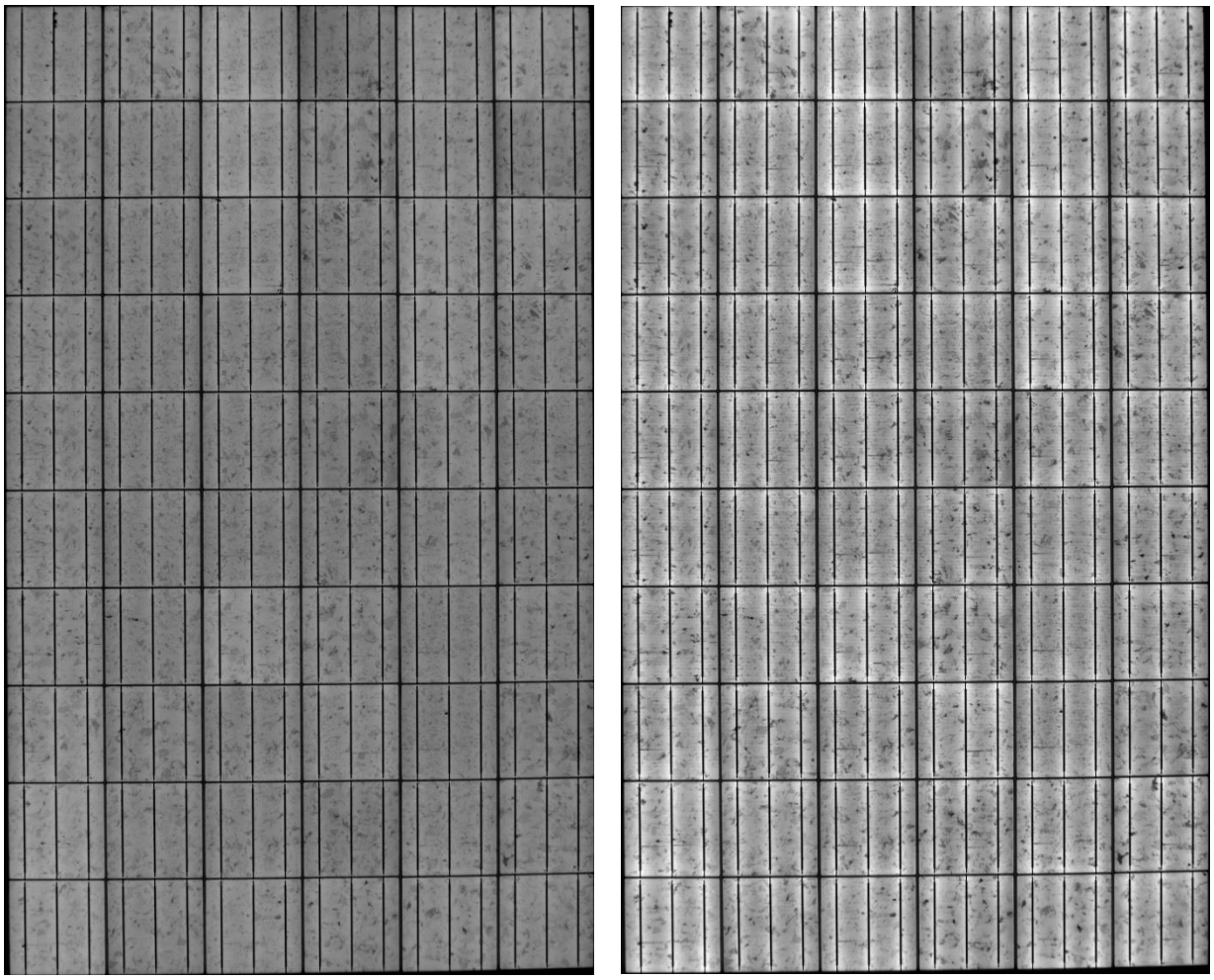

Figure C-7. EL images of Module #6. Left = low current, right = high current.

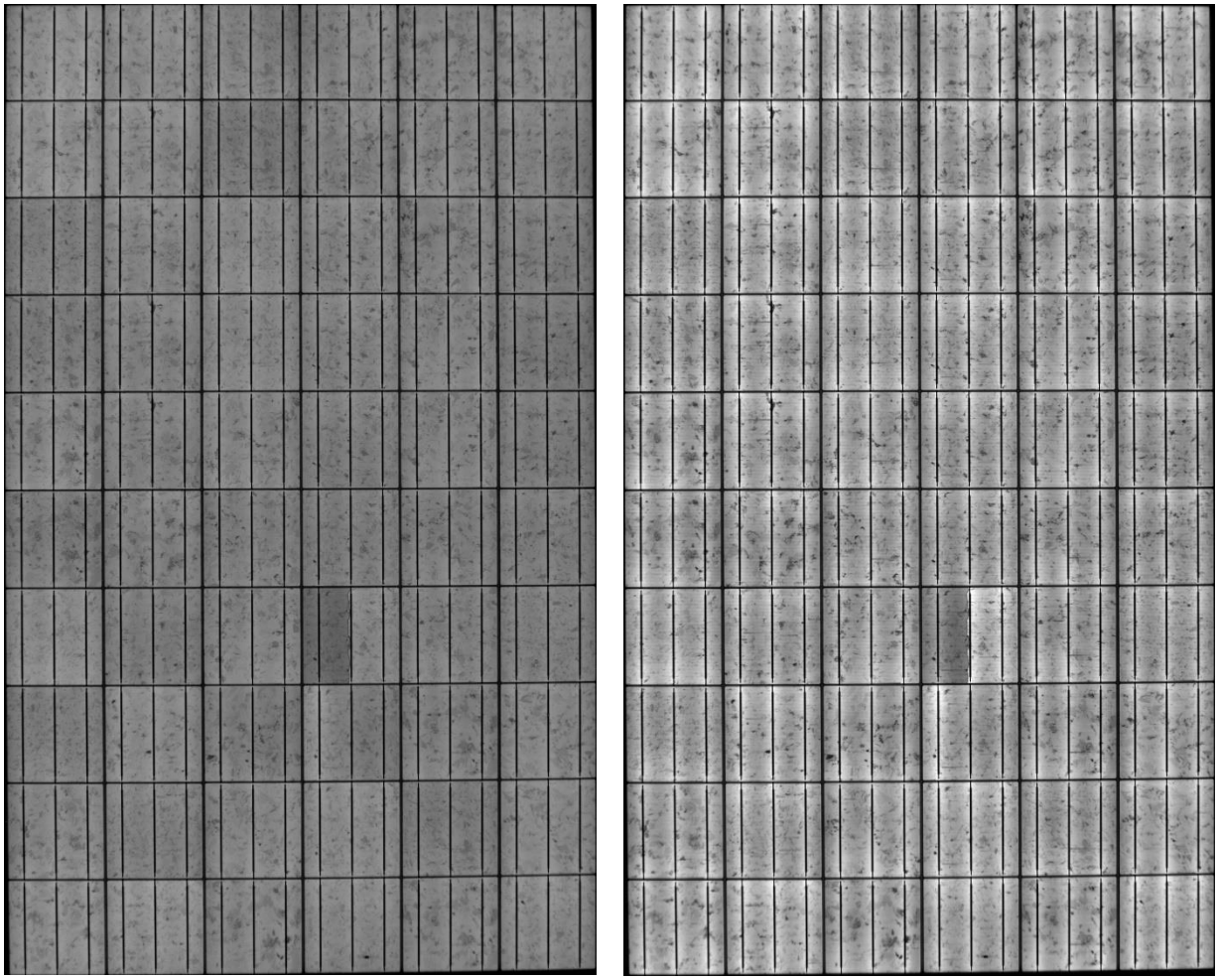

Figure C-8. EL images of Module #7. Left = low current, right = high current.

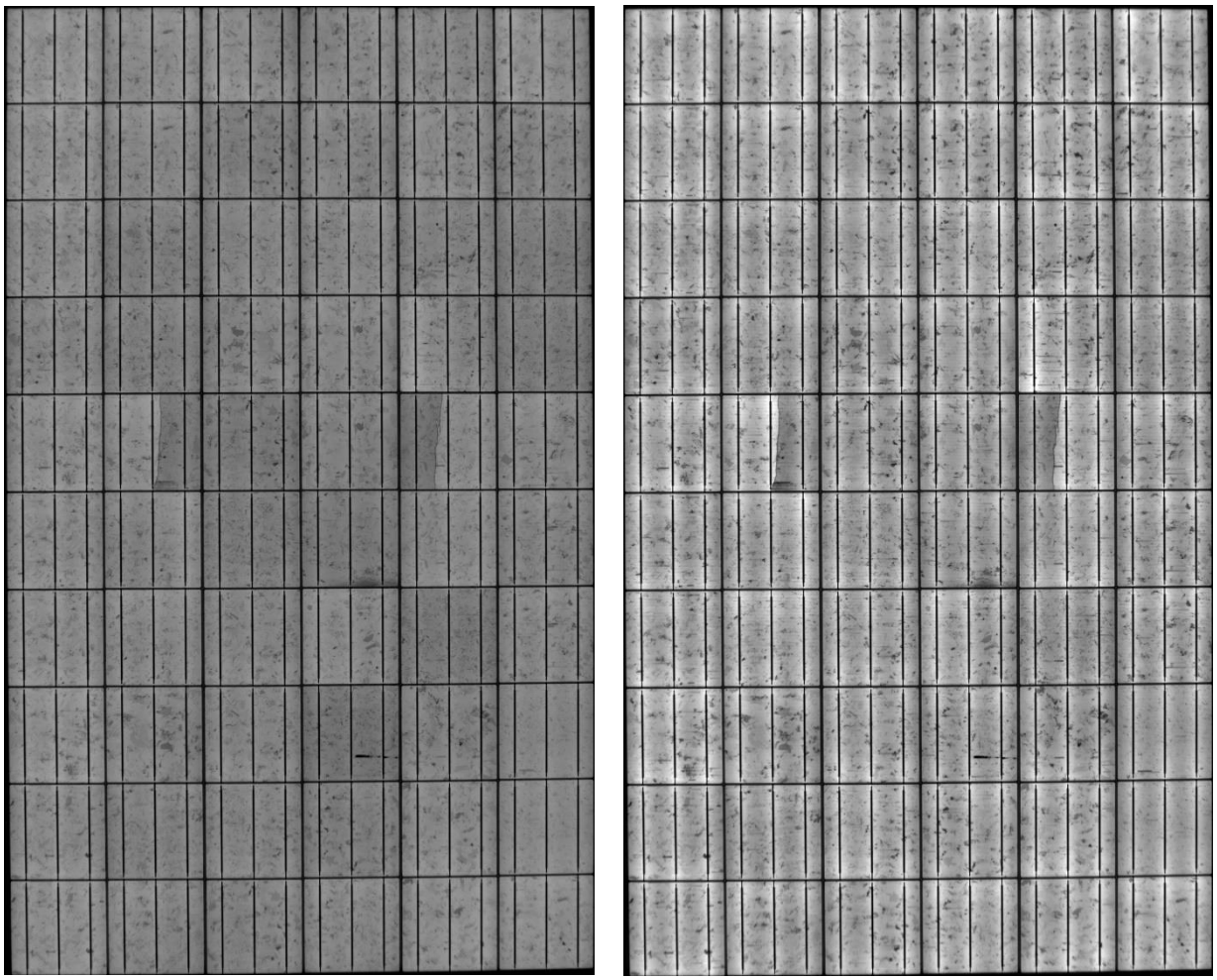

Figure C-9. EL images of Module #8. Left = low current, right = high current.

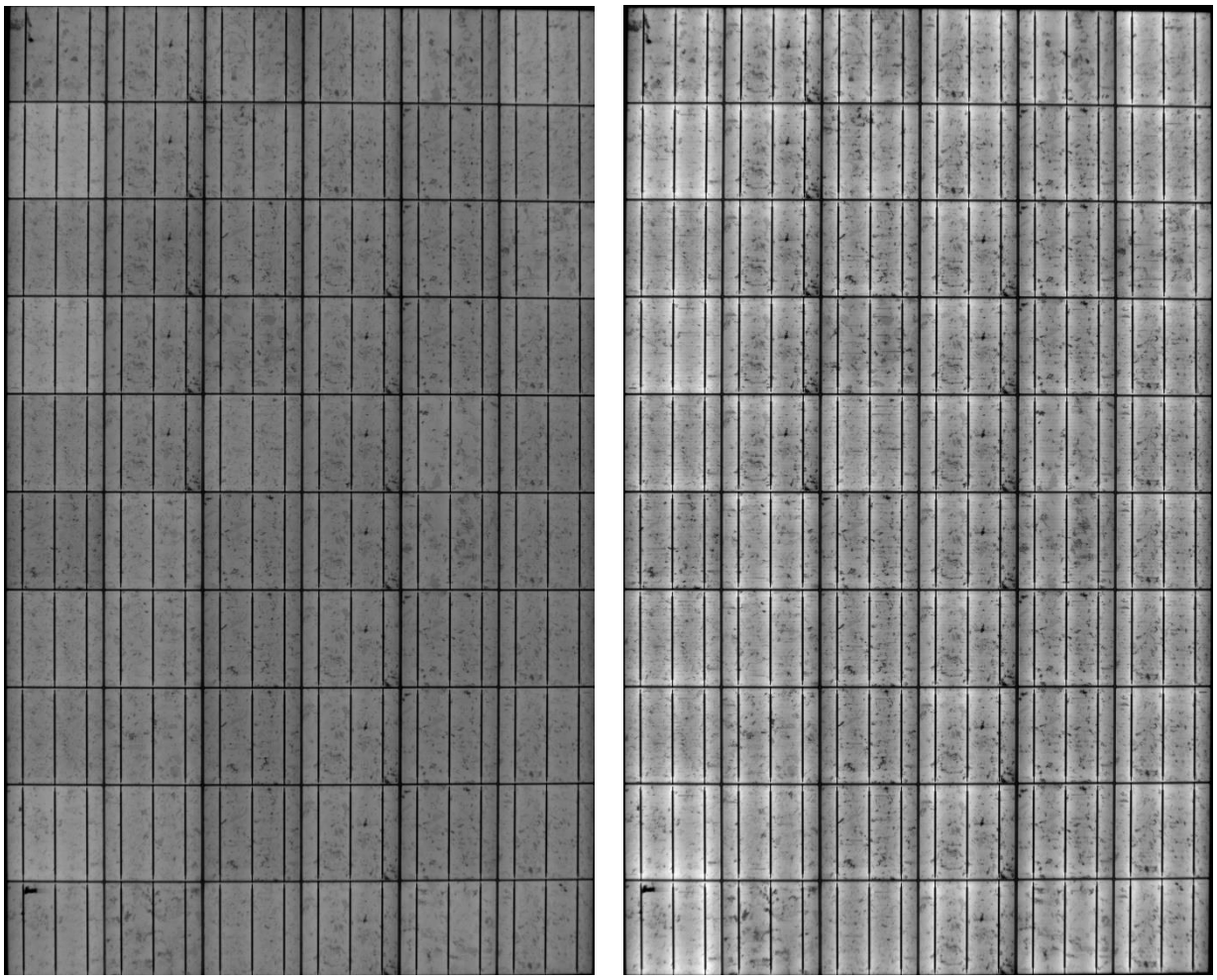

Figure C-10. EL images of Module #9. Left = low current, right = high current.

C.4. Conclusions

The flash I-V tests and EL imaging support the conclusion that the simulated HEMP exposure did not lead to any discernable immediate impacts on PV module performance. In other words, within the limits of this experiment, the results indicate that the EMP exposure did not cause any damage to the modules that led to an immediately-observable impact in electrical performance.

It would be of value to place these modules under sun in the PSEL or a similar facility and monitor them for a period of months to see whether the EMP exposure leads to any changes in long-term degradation of these modules.

DISTRIBUTION

Email—Internal

Name	Org.	Sandia Email Address
Tyler Bowman	01353	tbowma@sandia.gov
Jack Flicker	08812	jdflick@sandia.gov
Ross Guttromson	08812	rguttro@sandia.gov
Matthew Halligan	01353	mhallig@sandia.gov
Rodrigo Llanes	01353	rllanes@sandia.gov
Michael Ropp	08812	meropp@sandia.gov
Bruce King	08824	bhking@sandia.gov
Charles Robinson	08824	cdrobin@sandia.gov
Charles Hanley	08810	cjhanle@sandia.gov
Steven Glover	01353	sfglove@sandia.gov
Luis San Martin	01352	lsanmar@sandia.gov
Salvatore Campione	01352	scampi@sandia.gov
Summer Ferreira	08812	srferre@sandia.gov
Technical Library	01977	sanddocs@sandia.gov

This page left blank

Sandia National Laboratories is a multimission laboratory managed and operated by National Technology & Engineering Solutions of Sandia LLC, a wholly owned subsidiary of Honeywell International Inc. for the U.S. Department of Energy's National Nuclear Security Administration under contract DE-NA0003525.